SOFT AND SKIN-LIKE STRETCHABLE SILK-BASED EPIDERMAL ORGANIC BIOELECTRONICS FOR COMPREHENSIVE HUMAN PHYSIOLOGICAL SIGNAL MONITORING

by
SEYED SAJJAD MIRBAKHT

Submitted to the Graduate School of Engineering and Natural Sciences
in partial fulfilment of
the requirements for the degree of Master of Science

Sabancı University
July 2024

ABSTRACT

SOFT AND SKIN-LIKE STRETCHABLE SILK-BASED EPIDERMAL ORGANIC BIOELECTRONICS FOR COMPREHENSIVE HUMAN PHYSIOLOGICAL SIGNAL MONITORING

SEYED SAJJAD MIRBAKHT

ELECTRONICS ENGINEERING M.Sc. THESIS, July 2024

Thesis Supervisor: Assoc. Prof. Dr. Murat Kaya YAPICI

Keywords: biosignals, biomaterials, flexible electronics, silk, soft electronics

Skin-like epidermal bioelectronics, which emerged as a unique and transformative technology, offers highly imperceptible and wearable, soft digital health units mechanically akin to human skin for continuous and real-time health monitoring. These innovations, stemming from advancements in novel material synthesis and fabrication techniques, offer unparalleled features such as conformability, miniature footprint, and elasticity, where such unique features not only enhance the precision of health data recording but also promote patient adoption due to their comfort and unobtrusiveness. However, existing solutions still lack desirable properties, such as self-adhesivity, breathability, biodegradability, and transparency, and fail to offer a streamlined and scalable fabrication process. This thesis addresses the shortcomings in the current state-of-the-art by presenting protein-based silk-based skin-like epidermal bioelectronics, exploiting all the desirable material features of silk as a substrate, which have been individually present in existing devices but never combined into a single embodiment. As a significant advancement, the all-in-one solution presented in this thesis demonstrates excellent self-adhesiveness (300 N/m), high breathability (1263 g.h-1.m-2), and rapid biodegradability in soil within a mere two days. Additionally, possessing an elastic modulus of ~ 5 kPa and surpassing 600% in stretchability, the silk-based, biodegradable soft electronics seamlessly replicate the mechanics of the epidermis and form a conformal skin/electrode interface. Therefore, precisely inkjet-patterned with silver nanoparticle inks and coupled with a flexible readout circuitry, silk epidermal bioelectronics is capable of real-time and non-invasive recording of electrophysiological signals, including cardiac (ECG), neural (EEG), muscular (EMG), and ocular (EOG)

biopotentials, in durations reaching up to 12 hours with superior performance in par with Ag/AgCl gold standard, “wet” electrodes.

ÖZET

KAPSAMLI INSAN FIZYOLOJIK SINYAL IZLEME IÇIN YUMUŞAK VE DERI GIBI ESNEK IPEK BAZLI EPIDERMAL ORGANIK BIYOELEKTRONIKLER

SEYED SAJJAD MIRBAKHT

ELEKTRONIK MÜHENDISLIĞI YÜKSEK LİSANS TEZİ, TEMMUZ 2024

Tez Danışmanı: Doç. Dr. Murat Kaya YAPICI

Anahtar Kelimeler: biyopotansiyel takibi, biyomalzemeler, esnek elektronikler, ipek yumuşak elektronikler

Benzersiz ve dönüştürücü bir teknoloji olarak ortaya çıkan deri gibi epidermal biyoelektronik, sürekli ve gerçek zamanlı sağlık takibi için mekanik olarak insan derisine benzeyen, son derece algılanamaz ve giyilebilir, yumuşak dijital sağlık birimleri sunmaktadır. Yeni malzeme sentezi ve üretim tekniklerindeki ilerlemelerden kaynaklanan bu yenilikler, uyumluluk, minyatür ayak izi ve esneklik gibi benzersiz özellikler sunmakta ve bu benzersiz özellikler yalnızca sağlık verilerinin kaydedilmesinin hassasiyetini artırmakla kalmayıp aynı zamanda konforu ve göze batmaması nedeniyle hastaların benimsemesini de teşvik etmektedir. Bununla birlikte, mevcut çözümler hala kendinden yapışkanlık, nefes alabilirlik, biyolojik olarak çözünebilirlik ve şeffaflık gibi arzu edilen özelliklerden yoksundur ve kolay ve ölçeklenebilir bir üretim süreci sunamamaktadır. Bu tez, ipeğin mevcut cihazlarda ayrı ayrı bulunan ancak hiçbir zaman tek bir düzenlemede birleştirilmemiş olan tüm arzu edilen malzeme özelliklerini bir alt tabaka olarak kullanan protein bazlı ipek bazlı deri gibi epidermal biyoelektronikler sunarak mevcut en son teknolojideki eksiklikleri ele almaktadır. Önemli bir ilerleme olarak, bu tezde sunulan hepsi bir arada olan çözüm,

mükemmel kendinden yapışkanlık (300 N/m), yüksek nefes alabilirlik (1263 g.h-1.m-2) ve sadece iki gün içinde toprakta hızlı biyolojik çözünürlük göstermektedir. Ayrıca, ~5 kPa'lık bir elastik modüle sahip olan ve esneme kabiliyeti %600'ü aşan ipek bazlı, biyolojik olarak çözünebilir yumuşak elektronikler, epidermisin mekaniğini sorunsuz bir şekilde taklit etmekte ve konformal bir cilt/elektrot arayüzü oluşturmaktadır. Bu nedenle, gümüş nanopartikül mürekkeplerle hassas bir şekilde mürekkep püskürtmeli olarak desenlendirilen ve esnek bir okuma devresiyle birleştirilen ipek epidermal biyoelektronik, Ag/AgCl standart, "ıslak" elektrotlarla eşit üstün performansla 12 saate kadar ulaşan sürelerde kardiyak (EKG), nöral (EEG), kas (EMG) ve oküler (EOG) biyopotansiyeller dahil olmak üzere elektrofizyolojik sinyallerin gerçek zamanlı ve invazif olmayan kaydını yapabilmektedir.

ACKNOWLEDGEMENTS

Hereby, I would like to extend my sincerest and deepest gratitude to my advisor, Prof. Murat Kaya Yapici, for his mentorship and great support. As a master's student, throughout the past two years, he has consistently trusted in the ideas I formulated, providing me with the courage and motivation to pursue them. He has guided me technically through the engineering obstacles I faced and facilitated access to any tools and materials necessary to realize those ideas. In a relatively short period, all the achievements, from various scientific papers to prospective innovative and game-changing ideas, would not have been possible in any other environment - something which makes me feel both fortunate and proud! What I would like to deeply acknowledge and underscore is the foundation of respect, understanding, and care that he expressed to all of his students. Any feelings and concerns were listened to with patience and respect, and the best solutions were offered with sympathy and kindness. Conspicuous mistakes were not patronized but were regardfully corrected. Unrefined ideas were not belittled but were met with alternative proposals. Where all of these factors collectively led to a research group with well-guided, motivated members, and innovative scientific outputs.

Words may not fully capture the depth of my gratitude, but I wish to express my heartfelt thanks to my parents. Their hearts have been in sync with my joys and sorrows throughout this journey. Those who have shown enthusiasm in listening to my ongoing scientific projects and have shared in the joy of my engineering endeavors. I also want to extend my acknowledgement to my dearest sisters, who are not only teachers by profession but have also been my first and foremost educators in life. I couldn't have come this far without you all.

Additionally, I extend my warmest appreciation to my dearest friend, *Furkan Pekel*. He has been a beacon of motivation during my lowest and most exhausting moments, encouraging me to persevere and not abandon my dreams. He was the sole person who witnessed the true extent of my relentless efforts and motivation, constantly reminding me that these endeavors will not go unrewarded.

Indelibly, I wish to express my gratitude to *Ata Golparvar*, a cherished friend, collaborator on numerous publications, and a mentor. He is someone from whom I have learned professionalism, perseverance, and patience. Thank you for your constant presence and support.

Lastly, I wish to extend my genuine appreciation to all the friends in our team, who I fondly refer to as my SU-MEMS family. Their support was a reliable constant, whether it was tackling a challenging scientific problem (*Özberk Öztürk*), providing motivation for athletic endeavors (*Osman Şahin*), infusing humor and positivity into our daily efforts (*Saygun Güler*), lending a listening ear during moments of exhaustion (*Melih Taşdelen*), offering creative solutions during experimental dead-ends (*Farid Irani*), assisting you in your illustrations (*Ali Hosseinpour Shafaghi*), encouraging you to pursue your dreams (*Eda Akar*), mentoring you in rugby (*Oğuz Albayrak*), reminding the critical deadlines (*Seba Nur Alhasan*), or assisting you in finding the materials you need (*Maryam Sepehri*). We reveled in our collective achievements and spurred each other towards excellence. Absent was the sense of competition and the desire to outdo one another; instead, we stood united, resilient in the face of adversity and embracing our diversity. You were, without a doubt, the best, my friends!

For anyone lying in their bedroom at 4am wondering

the universe,

love,

and the children in war!

TABLE OF CONTENTS

LIST OF TABLES

LIST OF FIGURES

LIST OF ABBREVIATIONS

CHAPTER I

INTRODUCTION

1.1. Motivation

Tracking human electrical biosignals holds significant importance for both medical professionals and engineers. For the former, it provides insights into biological events that aid in diagnosing health disorders. For the latter, it serves as an input for innovative human-computer interaction solutions and out-of-hospital health monitoring technologies. To meet the technological demands for enhanced convenience and biosignal accuracy, a new class of electronics, often referred to as ‘epidermal electronics’, has been proposed. This emerging field continuously offers alternatives to traditional ‘rigid’, ‘bulky’, and ‘cable-intensive’ devices used for recording biosignals by introducing ‘flexible’, ‘miniaturized’, ‘stretchable’, and ‘wireless’ characteristics. The primary motivation behind epidermal electronics is the stretchable and soft nature of skin, which necessitates electronic interfaces with similar properties and resolution to (1) enhance patient comfort, (2) reduce visibility, (3) simplify usage with smaller form factors, and most importantly, (4) enhance the accuracy of the collected information.

However, current scientific and commercial epidermal electronic solutions still fall short in achieving all desired objectives, from integrating all skin properties into these solutions, to addressing resource-intensive fabrication processes and post-disposal environmental issues. This work, with the same objectives, investigates materials and fabrication techniques that not only mimic the attributes of skin but also lowers the end-product cost for a wider population and minimize environmental pollution risk.

1.2. Synopsis of Findings and Achievements

This study introduces silk Bombyx mori cocoons as a natural raw resource that, upon correct synthesis and plasticization, can serve as an optimal substrate for epidermal electronics. This substrate exhibits unique material properties that have not been collectively achieved in previous works. The Ca^{2+}-modified silk-based substrates in this study demonstrated (1) significant stretchability, (2) transparency comparable to glass, (3) breathability surpassing that of skin, (4) water insolubility, (5) biodegradability with a rapid decomposition rate of two days in soil, (6) self-adhesivity on par with commercial adhesive tapes, and (7) easy detachment from skin following a simple wash and gentle scrub.

A notable accomplishment of this work involves the high-resolution patterning of silk films using scalable technologies. By employing inkjet-printing of silver nanoparticle (AgNP) on donor substrates and subsequently transferring them to silk substrates, patterns as fine as 200 μm were successfully printed on the silk for the collection of electrical signals from the skin.

Furthermore, the design and fabrication of miniaturized, flexible, battery-powered, and wireless electronic circuitry enabled seamless connection to the inkjet-patterned silk electrodes. This allowed for the reception, amplification, processing, and transmission of various human biopotential signals to a nearby smartphone.

A key achievement of this work was the resulting device's ability to track cardiovascular electrocardiography (ECG), muscular electromyography (EMG), ocular electrooculography (EOG), and neural electroencephalography (EEG) signals using the same electrodes and hardware, with the only difference being the electrode placement. A significant highlight underscoring the advanced performance of the proposed device was the recording of neural Beta waves from a single channel.

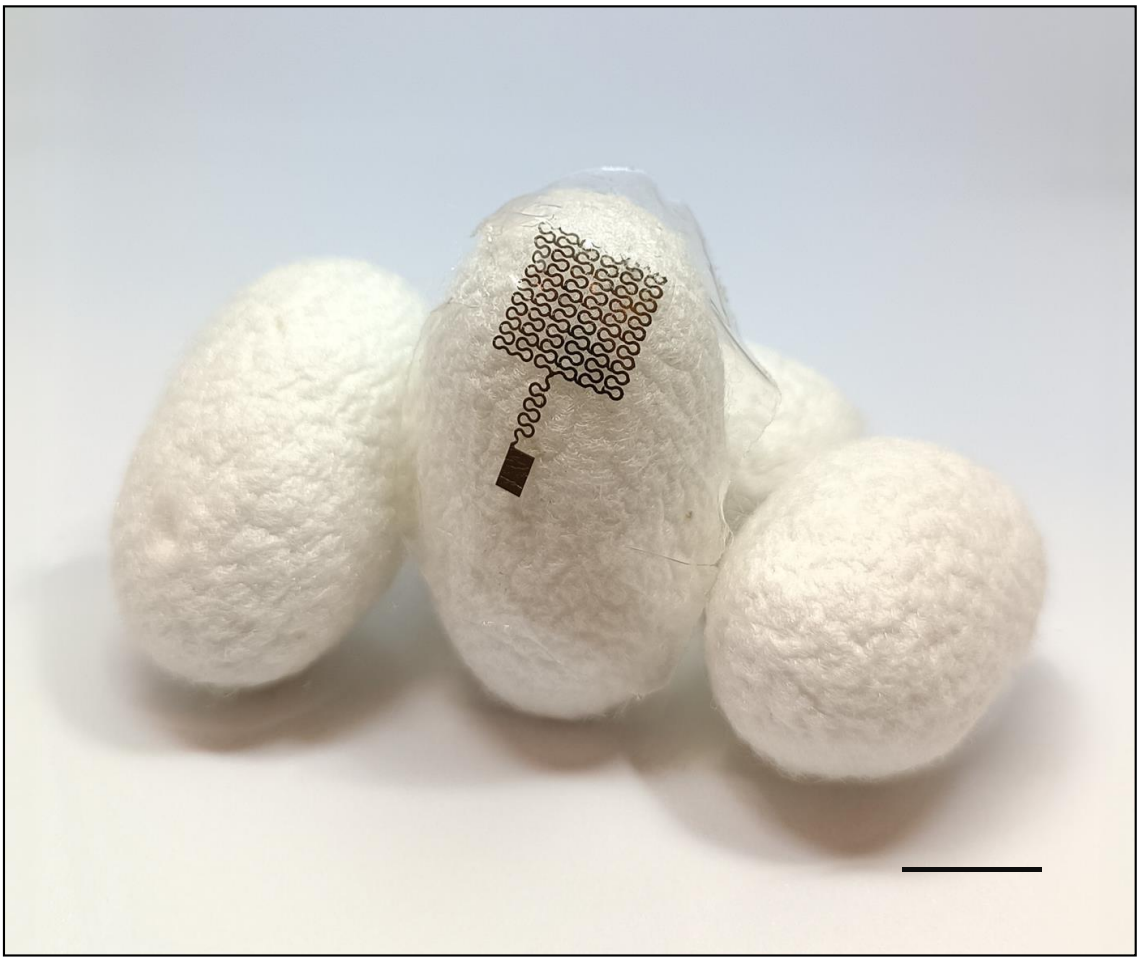

Figure 1.1. Photographic depiction of the silk-based silver inkjet-patterned soft electronic skin positioned on the original Bombyx mori silk cocoons. Scale bar, 1 cm.

1.3. Outline

In Chapter I, the motivation behind the fabrication of silk-based epidermal electronics is explored, ranging from the necessity of human biosignal tracking to the engineering approaches employed in the previous works. This chapter also delves into the significant discoveries and accomplishments of this work, including the innovative material properties of the proposed silk substrates, the high-quality and scalable patterning method that was utilized, the design of the biosignal recording hardware, and the range of human biopotential signals that can be acquired using the proposed cutting-edge solution.

In Chapter 2, we delve into the background of soft epidermal bioelectronics, emphasizing their critical distinctions from standard health monitoring rigid electronics. The primary objective in this chapter is to underscore the compelling motivation behind soft electronics as an alternative to existing solutions.

In Chapter 3, the experimental results of material characterization for soft silk films as a substrate are presented. These characterizations serve as a testament to the potential of the reported work for in vivo practical applications, while also considering post-disposal environmental impacts.

In Chapter 4, the potential of printing technologies, specifically inkjet printing, for patterning soft and elastic substrates using a straightforward print-and-transfer method is discussed. Additionally, the electrical performance of inkjet-patterned silver silk substrates is characterized. Finally, flexible and miniaturized data acquisition circuitry is introduced, which, when connected to such soft electronics, can find applications in a wide array of wearable health monitoring scenarios.

In Chapter 5, the various applications of soft silk-based electrodes in conjunction with flexible circuitry as an all-in-one wearable solution for recording human biopotential signals is presented. This chapter serves as a testament to the impact of the presented work in the wearable electronics domain by introducing the feasibility of collecting four distinct biopotential signals using identical hardware and electrodes. These signals range from cardiovascular to neural, demonstrating superior performance compared to their commercial counterparts.

CHAPTER II

BACKGROUND ON EPIDERMAL BIOELECTRONICS

2.1. Wearable Soft Epidermal Bioelectronics

Stretchable and soft epidermal electronics offer a versatile approach to non-invasive skin interfacing, enabling the acquisition of crucial physiological data or the delivery of therapeutic stimulation and medication [1]. In contrast to conventional rigid technologies, these platforms possess mechanical characteristics akin to the epidermis [2], and this seamless conformal interface is instrumental in high-fidelity biosignal acquisition while minimizing susceptibility to motion artifacts [3], [4], [5]. Within healthcare, their applications span a wide spectrum, encompassing the evaluation of skin thermal variations [6], innovative wound dressing techniques [7], monitoring skin hydration levels [8], assessing sleep quality [9], and detecting biomarkers directly on the skin surface [10]. In soft robotics, these devices have played a pivotal role in providing sensory feedback for prosthetic hands [11] and enabling electro-tactile stimulation for interactive human-robot interfaces [12]. Their utility extends further into self-powered electronic devices through energy harvesting methods [13], [14].

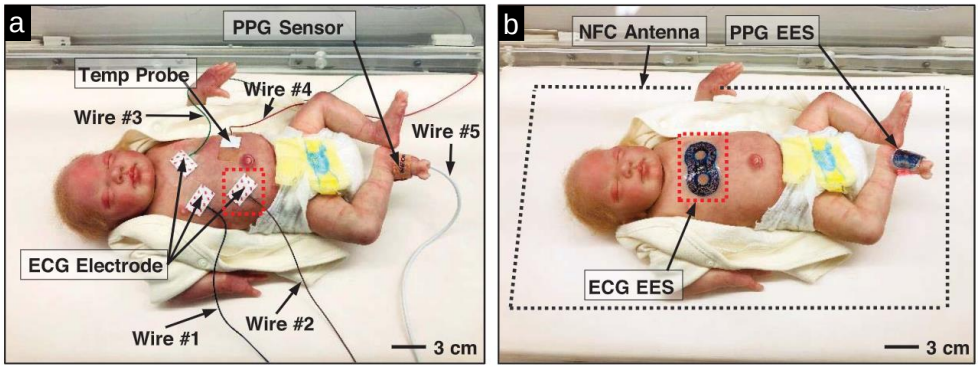

Figure 2.1. The transformative implications of epidermal electronics in health surveillance. (a) Contemporary technology employed for the observation of a neonate in a NICU environment, encompassing cardiography leads (positioned on the thorax) and a blood oxygenation probe (attached to the feet). (b) Soft and wireless electronic alternatives for the acquisition of ECG and PPG readings. Adapted with a CC BY 4.0 DEED license from [15]. Copyright © 2019, American Association for the Advancement of Science.

2.1.Limitations of Existing Models

The fabrication of skin-like bioelectronics, particularly those utilizing photolithography-based cleanroom procedures, has been instrumental in propelling the field forward. These microfabrication procedures generally share several steps, which include (1) the deposition of metals, (2) the application of photoresist through spin-coating, (3) UV exposure coupled with lithography, (4) etching of metal/resin, and (5) the lift-off process [16]. However, the potential for exploring alternative methods is hinted at by the intricate and resource-intensive nature of these processes, especially when applied to products designed for single use [17], [18]. Cleanroom processes demand a controlled environment, the establishment and maintenance of which can incur substantial costs and energy. The inherent complexity of these procedures may result in increased costs and challenges in maintaining precise control, potentially complicating the fabrication process and inflating the final product's cost, thereby limiting their accessibility for broader use [19], [20]. Given the unique opportunities presented by alternative,

cleanroom-free additive fabrication techniques such as inkjet-printing [21], screen-printing [22], gravure printing [23], and laser technologies [24], the transition of skin-like electronics from academic research prototypes to clinical-grade scalable technologies is feasible. Employing these fabrication and printing technologies, a diverse array of materials can be deposited and printed in the form of inks. However, when compared to microfabrication techniques, not all these materials may be compatible with standard processes and cleanroom environments. Furthermore, such printing methods, particularly screen-printing, are a favored choice for large-scale production due to their high throughput and relatively short processing time, comparable to microfabrication processes. This could potentially benefit a significant segment of the population as well as maintaining an environmentally friendly production cycle.

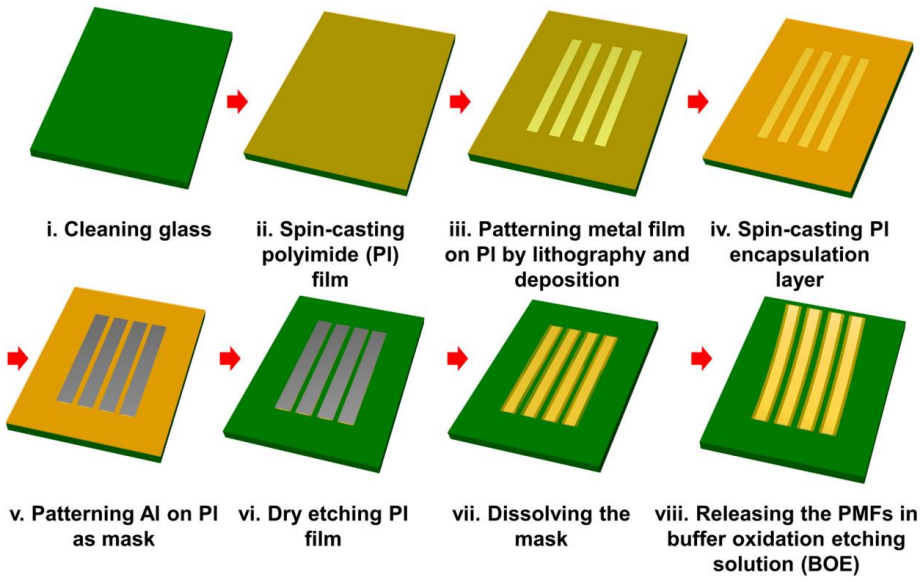

Figure 2.2. Typical microfabrication process necessary for the fabrication and patterning of epidermal bioelectronics. This includes multi-step spin-coating, photolithography, and etching. Adapted with a CC BY 4.0 DEED license from [25]. Copyright © 2021, American Association for the Advancement of Science.

In addition, concerns have also been raised regarding the environmental impact of chemically synthesized plastics and polymers such as polyurethane (PU), polydimethylsiloxane (PDMS), poly(vinyl alcohol) (PVA), and poly(3,4-ethylenedioxythiophene):poly(styrenesulfonate) (PEDOT:PSS) [26], [27], [28], [29],

[30], [31]. These materials often endure prolonged natural degradation when disposed of after a single use. Compounding this issue is the escalating volume of disposable electronics, contributing substantially to the burgeoning problem of electronic waste (e-waste), which is projected to reach a staggering 74 million tons by 2030 [32].

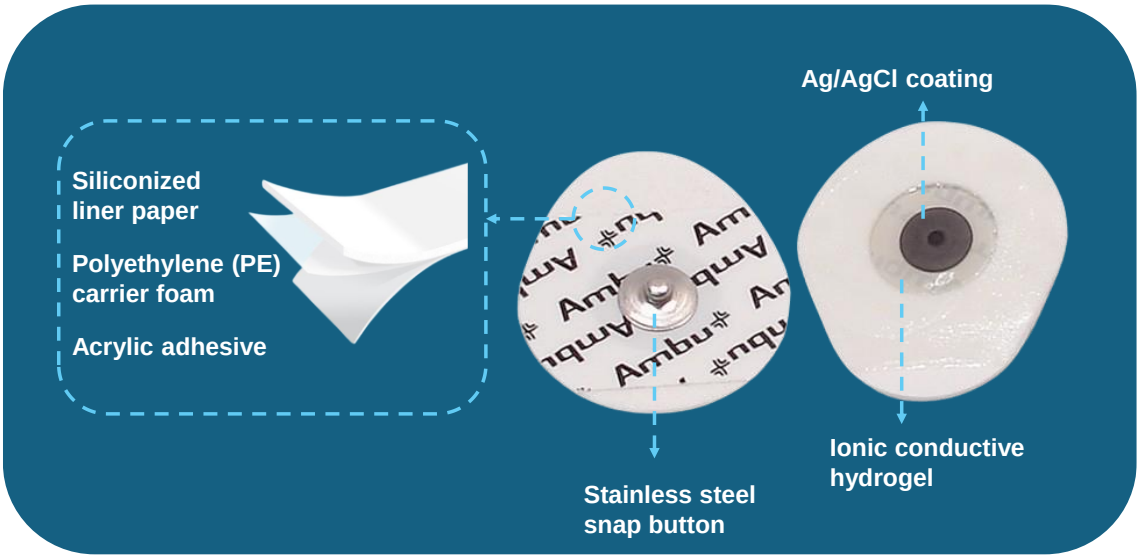

Figure 2.3. The Various Components of a Commercially Available silver/silver chloride (Ag/AgCl) Gel-Based Electrode. This includes plastic layers, which are not readily biodegradable and thus pose a potential environmental concern.

Another challenge shared between all skin-interfaced wearables persists in the limited biocompatibility of the skin-like bioelectronics, posing potential discomfort and dermatological irritation with extended use. Such discomfort may stem from using non-organic or potentially hazardous materials or disrupting the skin's natural trans-epidermal water loss and air permeation [33]. Furthermore, the continuous exposure of skin electronics to the natural deformation of the skin, sweat, and oils poses a significant challenge. Weak bonding between these devices and the skin often results in detachment, leading to performance issues such as data loss during signal recording and interruptions in continuous monitoring. This problem is particularly pronounced for skin electronics relying on low Van der Waals forces for adhesion, owing to their inherently lower adhesive energy [34].

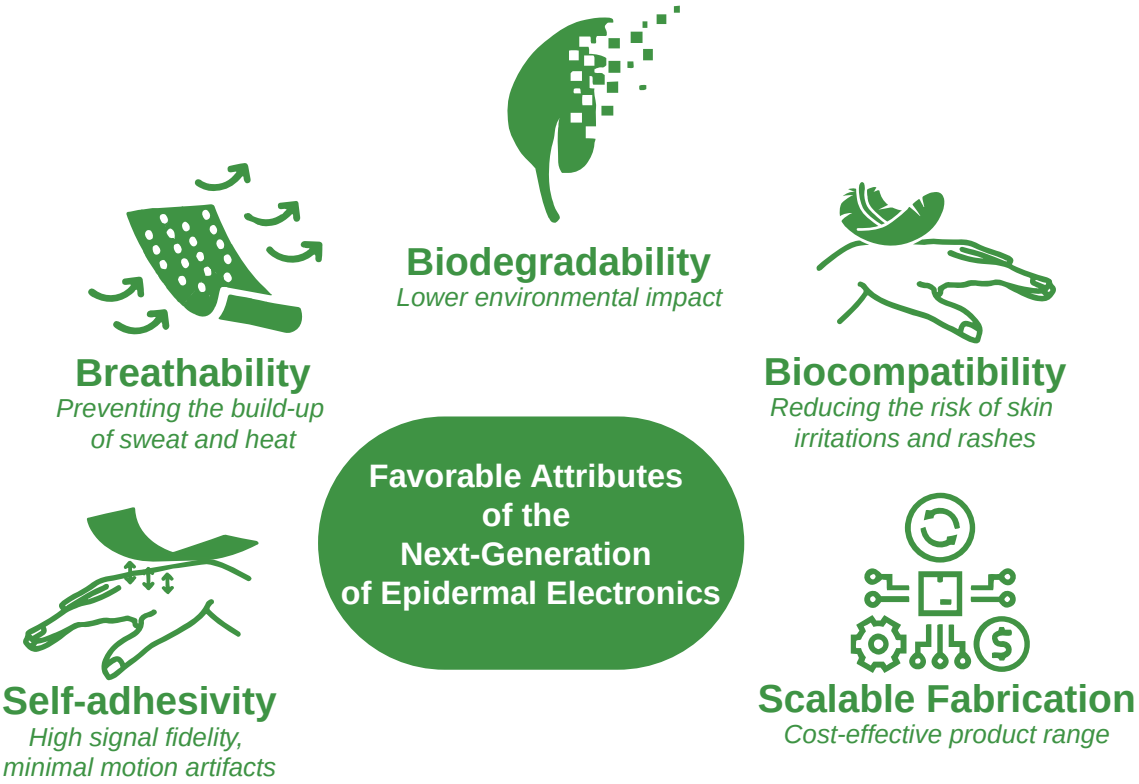

Figure 2.4. Desired material properties for enhanced performance in epidermal electronics. The properties include self-adhesivity, breathability, biodegradability, biocompatibility, and scalable fabrication that are collectively absent in existing works and reports.

2.2. Inkjet-Printing and Wearable Electronics

Inkjet printing is a highly efficient technique for the direct deposition of a variety of materials in the form of ink onto an array of substrates. This method is distinct from photolithography processes, which necessitate the use of physically pre-prepared masks. Conversely, inkjet printing employs digitally modifiable patterns, and this digital control over the printing process enhances the quality, speed, and precision of material deposition. Moreover, due to its straightforward processing, cost-effectiveness, and superior adaptability for large-scale fabrication of electronic devices, sensors, and light-emitting diodes, inkjet printing presents a compelling solution in both industrial and scientific settings.

For the printing process to be effective, certain fluid parameters of the ink, such as viscosity and surface tension, along with the particle size of the suspended functional materials within the ink, must be maintained within an optimal range. Each of these parameters, if not correctly optimized, could result in specific printing failures. For example, if the viscosity is not well-optimized, no ink would be ejected from the nozzles. Similarly, if the surface tension of the liquid exceeds the surface energy of the substrate, the high contact angle between the ejected ink and substrate will result in non-homogeneous printing. Furthermore, if the particle size of the ink is greater than or similar to the nozzle diameter, nozzle clogging could lead to printing failure.

The ejection of ink from the nozzles in inkjet printing typically relies on either thermal processes or piezoelectric principles. In both cases, droplets are ejected from the nozzle if the pressure on the fluid surpasses a certain threshold. In the absence of pressure, the liquid will remain at the nozzle due to surface tension. In the thermal method, an electric current is passed through a heater, causing the liquid to heat above its boiling point and form tiny bubbles. Upon removal of the current, the bubbles disappear due to heat transfer, and the rapid expansion and collapse of these bubbles generate a pressure pulse. In the piezoelectric method, the pressure is generated by applying an ultrasonic mechanical force from a piezoelectric transducer.

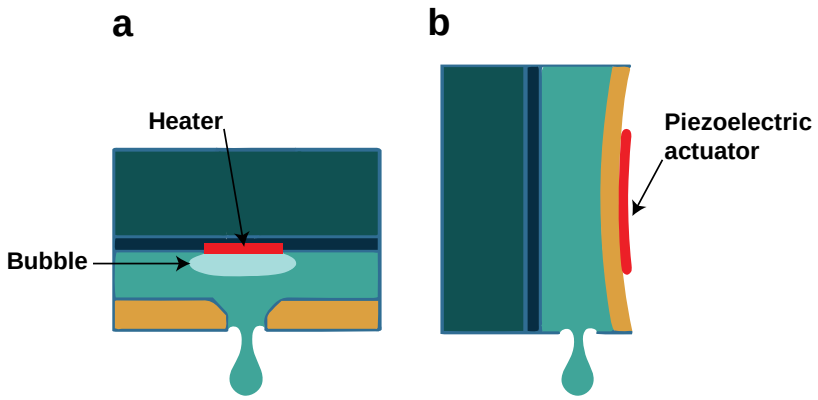

Figure 2.5. Inkjet-printing principles of (a) a thermal bubble jet print head and (b) a piezoelectrically actuated print head.

Inkjet printing technology has a significant role in the development of flexible and wearable electronic devices, precisely designed and for targeting human-health monitoring applications. Silver nanoparticle (AgNP), suspended in water-based or other organic solvents, proven their reliance and efficiency as inks for inkjet printing. Examples include wearable inkjet-printed AgNP-based Radio Frequency Identification (RFID) tags on tattoo papers [35], stretchable respiratory [36] and pressure sensors [37] on PDMS substrates, multifunctional printed devices on polyimide substrate [38], and individual tracking device on fabrics [39].

2.3. Biomaterials in Bioelectronic Applications

Protein-based natural biopolymers, including silk [40], cellulose [41], chitin [42], and lignin [43], are gaining recognition as robust biomaterials for the development of bioelectronics, owing to their inherent biocompatibility and widespread availability [43, 44]. Among mentioned, silk is a prime candidate for diverse medical applications due to its distinct natural structure, tunable mechanical properties [46], and degradation characteristics [47]. Various formats of silk, such as sponges [48], hydrogels [49], patches [50], and fibers [51], have been explored for applications in drug delivery [52], wound healing [53], and biosignal acquisition [54].

In medical applications, the core protein of silk undergoes a thorough extraction process, including removing the sericin component. Sericin, a set of soluble adhesive glycoproteins, coats the surface of fibroin, which is the primary protein targeted for synthesizing soft plastics. This sericin accounts for 25–30% of the total weight of the silkworm cocoon, and if not properly removed, it can trigger immune responses [55]. To eliminate sericin, silk cocoons are typically immersed in an aqueous solution of dissolved sodium carbonate (Na_2CO_3) and boiled for approximately 30 to 45 minutes [56]. Once this adhesive protein is removed, the fibroin fibers can be dissolved in an aqueous solution, paving the way for further processing into a variety of materials. Notably, Lithium bromide (LiBr) [57] and formic acid (CH_2O_2) [58] have been extensively employed in past procedures.

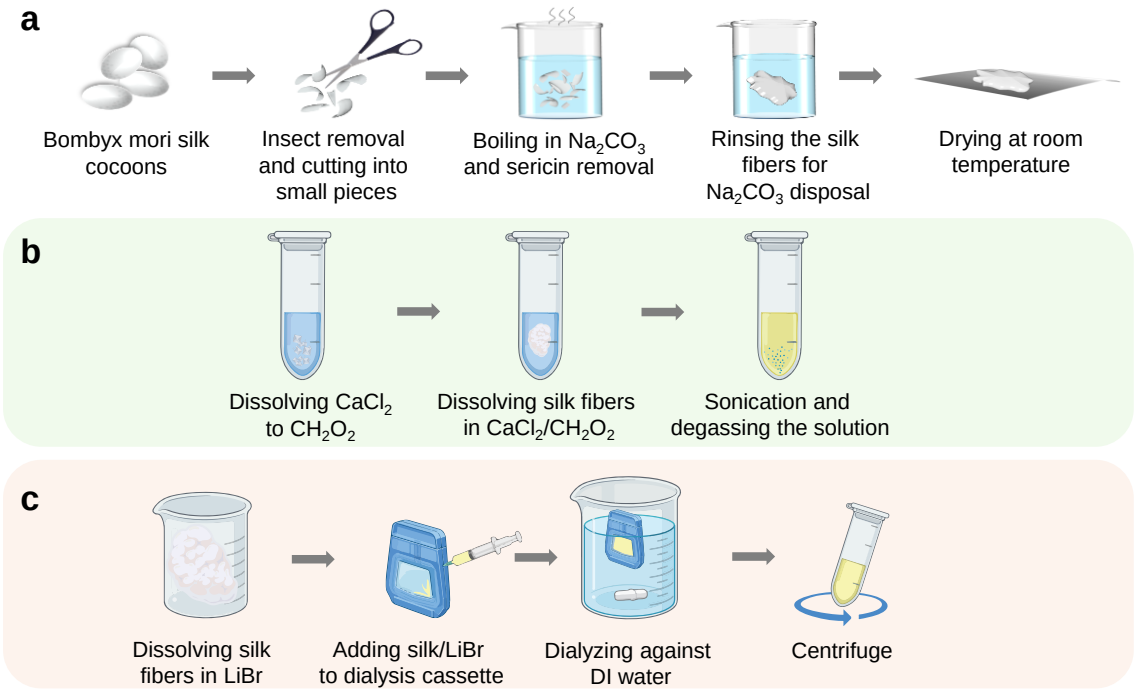

Figure 2.6. Procedure for synthesizing silk for biomedical applications. (a) the degumming process, which involves boiling silk cocoons in an aqueous solution of na_2co_3 to remove the sericin protein. (b) Dissolution of silk fibers using organic solvents, such as formic acid. (c) Dissolution of silk fibers in Lithium bromide, followed by additional steps including dialysis and centrifugation.

Recent advancements have precisely leveraged calcium ions (Ca^{2+}) to tailor silk properties, such as modulus, adhesiveness, and degradation rate, enhancing its suitability for skin-like electronics [46], [59], [60]. When tuned, these properties render silk an ideal substrate for such applications. For instance, the self-adhesive nature of silk-based skin-like bioelectronics plays a pivotal role in continuous physiological signal recording [61]. However, while robust adhesion is essential for accurate data capture, it can pose challenges, especially for individuals with delicate skin, such as the elderly and newborns. Their thinner skin layers and higher transepidermal water loss make their skin more susceptible to irritation and damage [62], [63], [64]. Balancing water solubility and adhesiveness through meticulous material property adjustments is key. This ensures adequate adherence of the electronics to the skin while enabling easy

removal through simple washing, thereby mitigating potential skin damage. Achieving this balance holds promise in preserving both the efficacy of data capture and the skin health of vulnerable individuals.

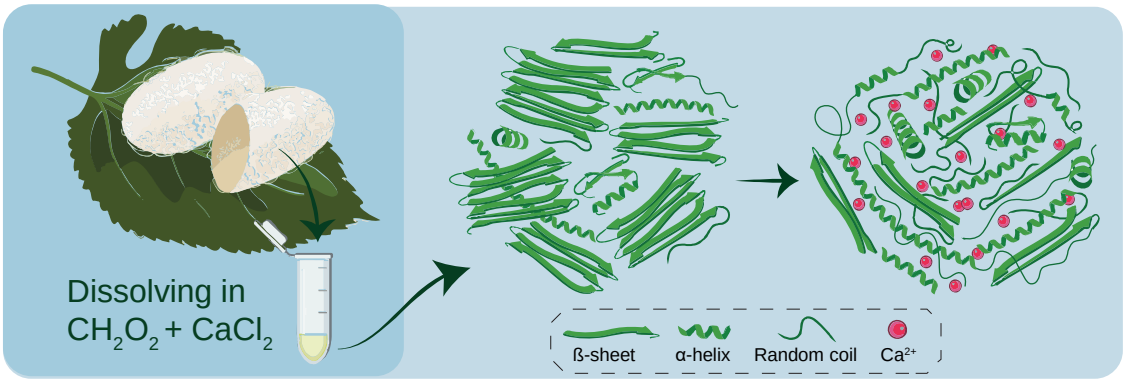

Figure 2.7. Schematic representation illustrating the effect of ca^{2+} on the protein structure transition from crystalline to amorphous.

2.4.Related works

In light of the broader implications of our study, it is noteworthy that silk composites with conductive fillers have been previously explored for human electrophysiological signals monitoring [65], [66]. However, they face fine-tuning challenges due to their mechanical properties and limited transparency. Similarly, silk films with deposited conductive materials have been studied [46], [54], [67], [68], [69], [70], [71] yet these efforts do not fully capitalize on the unique characteristics of silk, meticulously tuned and optimized to address the existing gaps in skin-electronic materials. Additionally, the precise patterning of silk films remains a challenge in these reported works due to limitations in fabrication methods. Table 2.1. provides a quantitative comparison between this work and previously reported silk-based wearable electronics for human physiological sensing.

Moreover, silk-based skin-like epidermal bioelectronics stand distinct from synthesized polymer-based materials. Indeed, other epidermal electronics with adhesive properties

often require a secondary separate adhesive polymer layer, [72], [73], [74], [75], [76], [77], [78], [79] complicating the fabrication process and adding cost and material usage. Fabrication processes based on microfabrication techniques being resource-intensive and necessitating a well-regulated environment, lead to substantial costs and intricacy in fabrication. This, in turn, results in high-priced final products, thereby restricting their widespread applicability [75], [76], [78], [80], [81]. Integrating conductive fillers into polymer matrices limits proper permeability and optical transparency [17], [82], [83]. Importantly, synthetic polymers and plastics lack natural decomposition, contributing to e-waste and environmental concerns [27], [84]. Table 2.2. provides a qualitative comparison between silk-based skin-like bioelectronics and various previously reported skin-like wearable bioelectronics, highlighting its unique advantages.

Table 2.1. Quantitative comparison between this work and previously silk-based wearable electronics for human physiological sensing.

Ref.	**Conductive Material**	**Deposition Technique**	**Resolution (µm)**	**ECG**	**EMG**	**EOG**	**EEG**	**Breathbility ($g.hour^{-1}.m^{-2}$)**	**Stretchability (%)**	**Young' s Modulus (MPa)**	**Biodegradability (days)**	**Transparency (%)**	**Adhesivenes (N/m)**	**Portability**
[67]	AgNW	Suction filtration	Not Applicable	☑	☑	✗	✗	106.3 (35 °C)	60	-	-	-	13 (on wet human skin)	✗
[68]	Polypyrrole (ppy)	Dip-coating	Not Applicable	☑	☑	✗	✗	-	> 100	79.62	~ 15	-	13.5 (on glass)	✗

[71]	[46]	[85]	[70]	[54]	[69]	[66]
AgNW	Gold (Au)	Graphene	Au Nanotrough	Polypyrrole (ppy)	CNT	PEDOT:PSS
Stencil-print	Thermal evaporation	Blend	Microfabrication techniques	Composite layer	Brushed	Blend
-	Not Applicable	Not Applicable	Not Applicable	Not Applicable	Not Applicable	Not Applicable
☑	✗	☑	✗	☑	☑	☑
✗	☑	✗	☑	☑	☑	☑
✗	✗	✗	✗	☑	✗	✗
✗	✗	✗	✗	☑	✗	✗
71.6 - 168.5 (50 °C)	-	-	-	-	-	~ 117 (37 °)
-	> 400	-	-	~ 300	~ 35	> 250
0.010 (50% RH)	1.66 (50% RH)	-	0.134	236 (~ 53 % RH)	-	~ 190
-	-	-	-	-	-	-
90	-	-	-	-	-	-
10 (on porcine skin)	90 (on human skin)	-	-	40 (at 94.6% RH on human skin)	-	-
✗	✗	✗	✗	✗	✗	✗

This work	AgNP	Inkjet printing	200	☑	☑	☑	☑	1262.6 (80 °C)	> 600	0.0051 (60% RH)	2	> 95	~ 300 (on glass)	✓

Table 2.2. Qualitative comparison between this work and previously reported various non-silk-based skin-like wearable bioelectronics for human physiological sensing.

Ref.	**Substrate**	**Conductive Material**	**Fabrication**	**Adhesive *[adhesivity source]***	**Breathable**	**Transparent**	**Biodegradble**	**ECG**	**EEG**	**EMG**	**EOG**
[72]	PDMS	Ag/AgCl/PEDOT:PSS	Stencil-printing	☑ *[PDMS-PEIE]*	✗	✗	✗	✓	✓	✓	✗
[73]	TPU	Ag/In/Ga/SIS	Contact-printing	☑ *[Acrylic adhesive]*	✗	☑	✗	✓	✓	✓	✓
[80]	Silicone elastomer	Cr/Au	Microfabrication	☑ [Self-adhesive]	✗	✗	✗	✓	✗	✗	✗
[74]	PET	CNT/PDMS/PEIE	✗	☑ *[PDMS-PEIE]*	✗	✗	✗	✓	✗	✗	✗
[75]	Ecoflex	Cr/Au	Microfabrication	☑ *[Adhesive silicone]*	☑	☑	✗	✓	✓	✓	✗
[76]	Silicone elastomer/PI	AgNP	Aerosol jet printing/ Microfabrication	☑ *[Adhesive elastomer]*	✗	✗	✗	✗	✗	✗	✓

[77]	TPU	AgNW	Dip-coating/ Laser cutting	☑ *[Liquid bandge]*	✗	☑	✗	✓	✗	✓	✗
[78]	PDMS	Galinstan (R)	Microfabrication	☑ *[Micropore commercial tape]*	✗	✗	✗	✓	✗	✗	✗
[83]	Silicone-based polymer	Carbon nanofiber/ Carbon black	Blend	☑ *[Self-adhesive]*	✗	✗	✗	✓	✓	✓	✗
[27]	PU nanomesh	Graphene	Electrospinning/ Laser scribing	✗	☑	✗	✗	✓	✓	✗	✓
[86]	TPU/WPU	Mxene-CNT	Electrospinning/ Spraying	☑ *[Self-adhesive]*	☑	✗	✗	✓	✓	✓	✗
[17]	Ecoflex	Silve microparticle	Blend	☑ *[Micropillar structure]*	✗	✗	✗	✓	✓	✗	✗
[82]	WPU	PEDOT:PSS	Blend	☑ *[Self-adhesive]*	✗	✗	✗	✓	✓	✓	✗
[81]	PEDOT:PSS	Graphene	Spin-coat/ Etching	✗	✗	☑	✗	✓	✓	✓	✓
[79]	PI/PDMS	AgNW	Laser cutting/ Spray printing	☑ *[PDMS]*	☑	☑	✗	✓	✗	✗	✗
This work	Silk	AgNP	Inkjet-printing	☑ *[Self-adhesive]*	☑	☑	☑	✓	✓	✓	✓

CHAPTER III

CHARACTERIZING THE MATERIAL PROPERTIES OF THE SYNTHESIZED SILK AS A SUBSTRATE FOR EPIDERMAL BIOELECTRONICS

3.1. Silk Solution Preparation

Natural *Bombyx mori* cocoons, ~ 4 cm long (purchased from a local vendor), were sectioned into ~ 1 cm^2 segments using stainless-steel scissors. To initiate the degumming process—the process to remove the sericin protein, a 40 mmol/l sodium carbonate solution was prepared by dissolving 8.48 g of Na_2CO_3 powder (Sigma-Aldrich, USA) in a 2-liter volume of deionized water. This solution was then elevated to a temperature of 100 °C under an aluminum foil seal in a 2-liter glass beaker. Subsequently, 10 g of the prepared cocoon segments were introduced into the boiling Na_2CO_3 solution and subjected to constant stirring for 45 minutes. After this treatment, cocoons were carefully withdrawn from the solution and thoroughly rinsed with deionized water. Excess water was removed by squeezing the cocoons. The treated cocoon segments were then rinsed in deionized water for 20 minutes to clear the residual sodium carbonate and sericin fully, and this was repeated three times. The treated cocoon segments were left to air dry overnight on aluminum foil within a fume hood. To prepare the 45 wt% $CaCl_2$/silk solution, 1.35 g of calcium chloride ($CaCl_2$, Sigma-Aldrich, USA) was mixed with 20 g of formic acid (CH_2O_2, Sigma-Aldrich, USA). This mixture was stirred until no visible $CaCl_2$ particles remained discernible. Following the dissolution of $CaCl_2$, 3 g of previously degummed cocoons was gradually introduced into the solution while the mixture was stirred at 700 rpm for 1 hour at room

temperature. Subsequently, the solution was transferred into an ultrasonication bath for 30 minutes at 45 °C to dissolve silk fibers further.

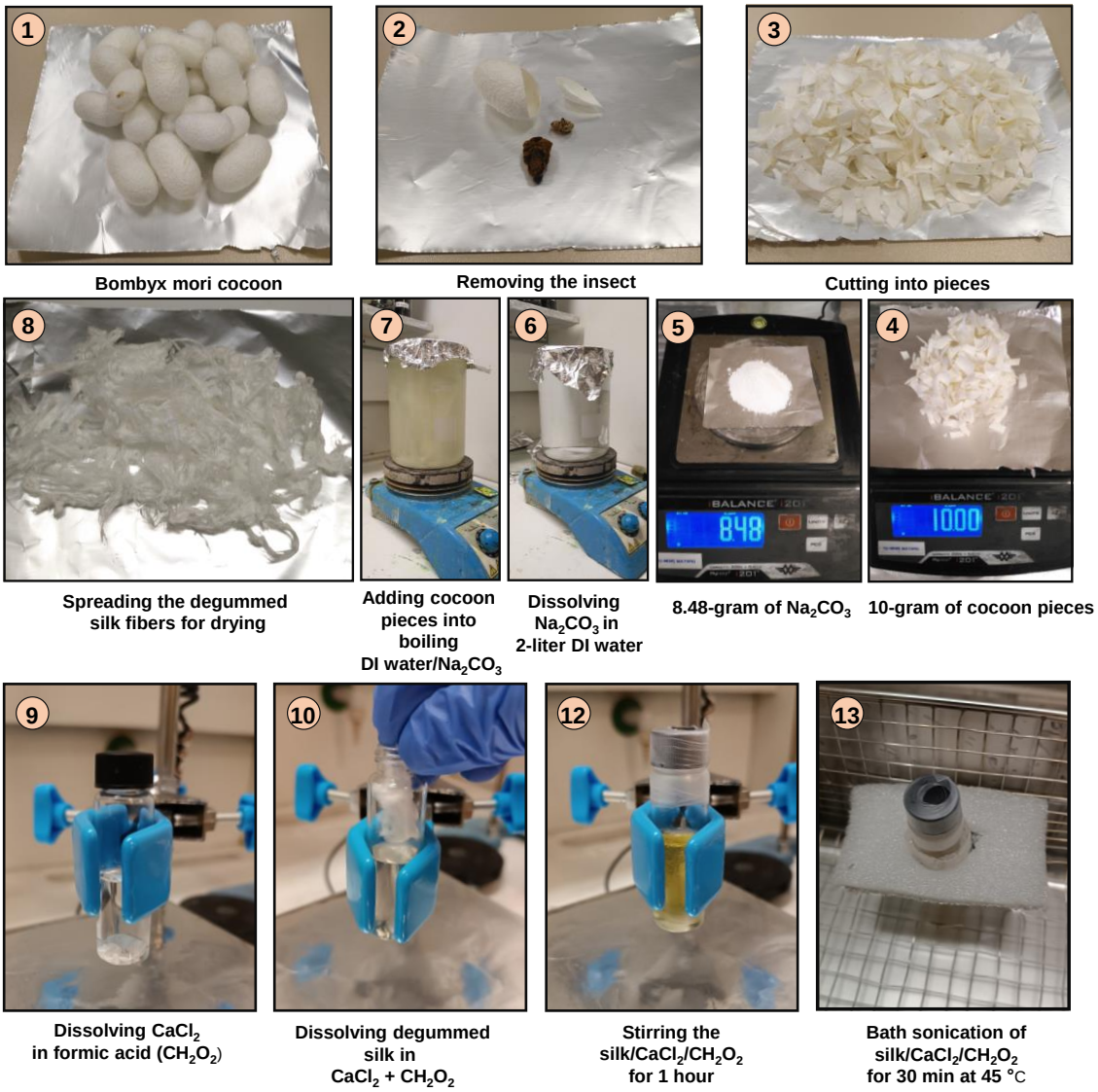

Figure 3.1. Process of degumming silk cocoons and silk solution preparation. The degumming process involves the following steps: 1) Procuring Bombyx mori cocoons. 2) Cutting the cocoons and removing the deceased insect. 3) Cutting the cocoons into approximately 1 cm2 pieces using stainless-steel scissors. 4) Weighing out 10 g of the cut cocoon pieces. 5) Preparing a 0.04 M Sodium carbonate (Na2CO3) solution, which requires 8.48 g of Na2CO3. 6) Dissolving Na2CO3 in 2 liters of DI water and bringing it to a boil. 7) Boiling the cocoon pieces in the DI water/Na2CO3 solution for 45 minutes. 8) Thoroughly rinsing the degummed silk fibers with fresh DI water and allowing them to dry overnight in a fume hood. The silk solution preparation involves:

9) Dissolving calcium chloride ($CaCl_2$) in formic acid (CH_2O_2) using a magnetic stir bar. 10) Adding the degummed silk fibers to the $CaCl_2/CH_2O_2$ solution. 11) Stirring the silk/$CaCl_2/CH_2O_2$ solution for 1 hour using a magnetic stir bar. 12) Bath sonication of the silk/$CaCl_2/CH_2O_2$ solution for 30 minutes at 45°C.

3.2. Formation of Skin-like Silk Bioelectronic

First, the 130 µm polyethylene terephthalate (PET) films were cleaned using isopropanol alcohol and deionized water and then dried using a nitrogen gun. Next, the surface wettability of the films was improved through a 1-minute corona treatment to enhance ink adhesion to the plastic surfaces (BD-20AC, Electro-Technic Products, USA). The inkjet printing of silver nanoparticles ink (AgNP, JS-A102A, Novacentrix, USA) was carried out employing an inkjet printer (DMP-2850, Fujifilm, USA) equipped with a loaded cartridge (Samba Dimatix, Fujifilm, USA), which featured twelve nozzles capable of jetting a minimum drop volume of 2.4 pL. A drop spacing of 15 µm was configured to ensure optimal print quality and electrical conductivity. The jetting process was executed under the following conditions: nozzle voltage of 30 V, nozzle temperature of 28 °C, and a jetting frequency of 10 kHz. The default Fujifilm Model Fluid waveform was applied to the piezoelectric elements, resulting in a calculated drop velocity of 6.6 m/s, and all the patterns were printed in a single printing cycle. Subsequently, the printed AgNP patterns were annealed at 140 °C for 20 minutes. Later, the as-printed serpentine AgNP network was transferred onto silk films by drop-casting silk solution onto the newly patterned PET substrates. We have experimentally found that to achieve a silk film thickness of 100 µm, a volume of 50 µL/cm^2 of the silk solution was required to be drop-casted. After applying the silk solution onto the donor substrates, each sample underwent vacuum desiccation to ensure no visible air bubbles remained within the silk solution. Finally, the samples were left to dry for 20 hours within a fume hood, allowing for the complete evaporation of formic acid. Next, a post-baking step was performed to detach the PET substrate from the silk/AgNP layers and enhance the peeling process for 45 wt% $CaCl_2$/silk films with a thickness of 100 µm. This thermal treatment involved heating the samples at 75 °C for 15 minutes in an oven.

These parameters are empirically optimized to achieve the most effective peeling process, which ensures that the force required to separate the elastic silk from the donor substrate does not push the silk into its plastic deformation region. Subsequently, the separated silk films, now patterned but still rigid, were subjected to a humidity treatment for 15 minutes within a controlled humidity chamber with a moisture level of 70% RH. This treatment restored the silk substrate to its initial soft and stretchable state, forming the skin-like silk bioelectronic patch.

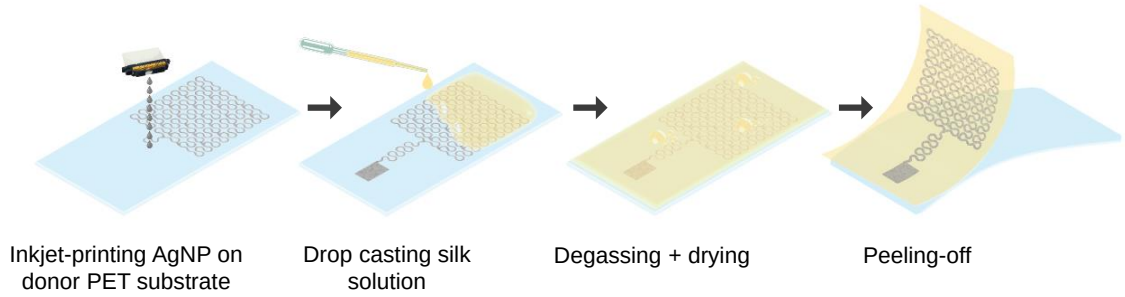

Figure 3.2. Fabrication process of inkjet-patterned silk bioelectronics.

3.3.Mechanical Properties of the Synthesized Silk Substrates

The mechanical properties of the silk films were fine-tuned through the controlled introduction of $CaCl_2$ to the silk fibroin fibers, which enabled their transformation into ultra-soft and imperceptible substrates for epidermal bioelectronics. Tensile tests were conducted on the fabricated silk films with varying $CaCl_2$/silk weight ratios formulation with a Universal testing meachine (UTM) (Zwick Z100, Germany). For each composition, 5 samples were tested (30 samples were investigated). The tests were conducted at a speed of 20 mm/min. The specimens were fabricated in an L-shape configuration, featuring a width of 20 mm, a thickness of approximately 200 μm, and an effective length of 40 mm. The Young's modulus was determined based on the data slope in (Δfore/Δstrain) the initial 0.5% strain region. The Young's modulus of the silk films exhibited a significant reduction, decreasing from 11.4 MPa to 427.1 kPa, as the $CaCl_2$ to silk weight ratio increased from 5 wt% to 50 wt% at a relative humidity of ~ 45% RH (Figure 3.3a). Correspondingly, the stretchability of the silk films increased

substantially, expanding from a mere 6% to an impressive >250% (Figure 3.3b). However, the silk films loaded with 50 wt% $CaCl_2$, despite their lower modulus of elasticity, were found to be mechanically unstable as a stand-alone solid substrate. Under ~ 45% humidity, they exhibited properties akin to a gel, rendering them impractical as a structural support for attachment onto the skin. In contrast, silk films loaded with 45 wt% $CaCl_2$ maintained superior mechanical characteristics, featuring Young's modulus of 501.1 kPa and stretchability of >230%. These properties closely matched the mechanical attributes of human skin, specifically the epidermis (which typically has a modulus ranging from 140 to 600 kPa [87], [88]). Consequently, the subsequent experiments in this study were conducted using silk films loaded with 45 wt% $CaCl_2$.

The influence of ambient humidity on the silk films is of notable significance, given that silk can absorb more water molecules as the Ca^{2+} ion content increases. For instance, the modulus of the 45wt% $CaCl_2$/silk films decreased from 501.1 kPa to 5.1 kPa, and the stretchability increased from >230% to >600% as the ambient humidity rose from ~45% to ~60% RH (Figure 3.3c-e). This phenomenon represents an additional adjustable parameter for fine-tuning the elasticity of Ca^{2+}-modified silk films.

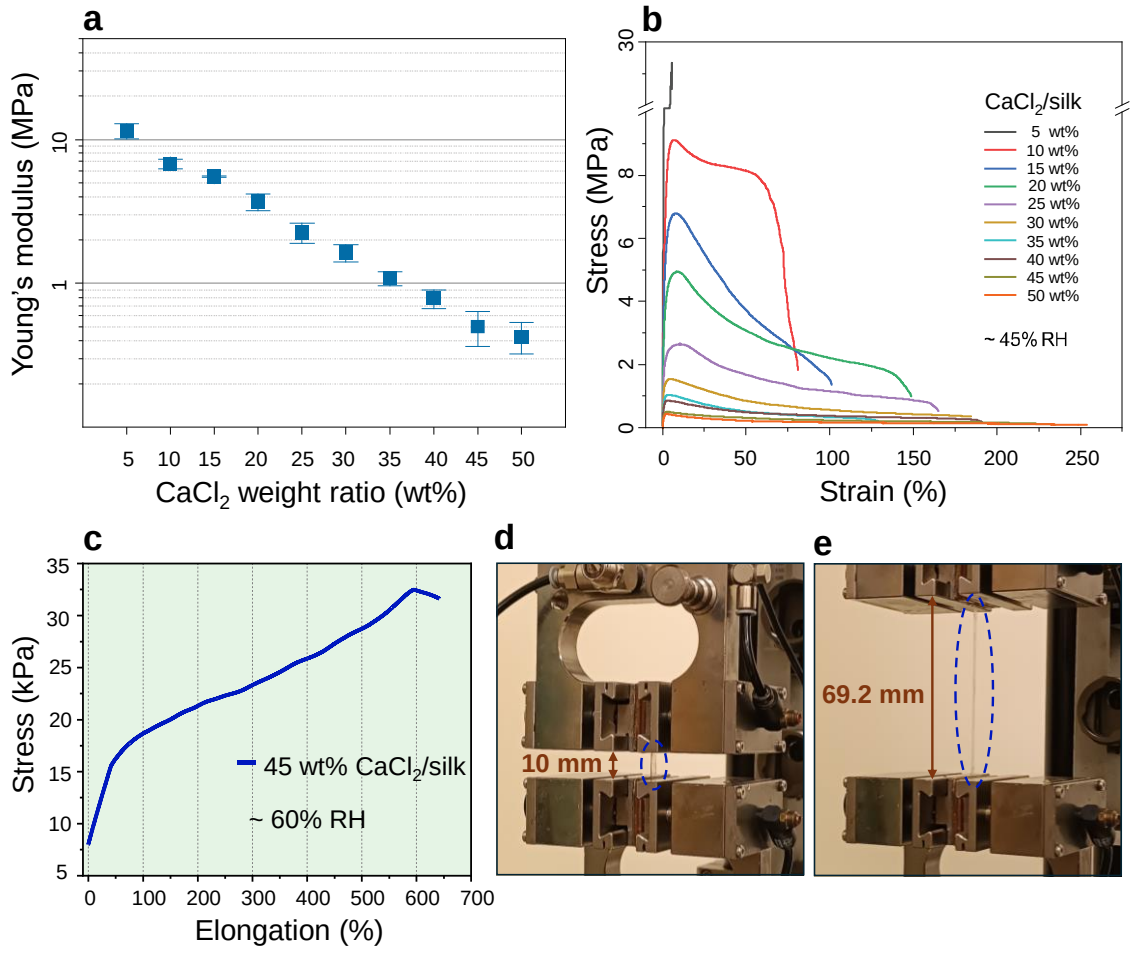

Figure 3.3. Mechanical characterization of silk as a soft substrate for skin-like bioelectronics (a) The Young's modulus of the silk substrate corresponding to different $CaCl_2$ values at a relative humidity of ~ 45%. (b) Stress-strain curves for silk films modified with varying concentrations of $CaCl_2$, ranging from 5 wt% to 50 wt%. The tests were conducted under approximately 45% relative humidity conditions. The curves demonstrate an increase in stretchability as the concentration of $CaCl_2$ increases. (c) The resulting tensile stress-strain graph of the silk demonstrated an elongation exceeding 600% under a 60% RH humidity condition. (d) The 45 wt% $CaCl_2$/silk film was attached to a mechanical testing machine with an initial length of 10 mm, and (e) it stretched to a length of 69.2 mm, indicating an elongation of 592%.

3.4.Material Characterization of the Synthesized Silk Substrates

3.4.1 Hygroscopic Properties of Silk: Heat-Induced Dehydration and Subsequent Rehydration

Silk films show revertability to their original form by reabsorbing water content after experiencing water loss. In the case of 45 wt% $CaCl_2$ loaded silk, a weight loss of 7.6% was observed following a 2-hour exposure to 75°C. Remarkably, this weight loss was fully recovered after 19 hours, and the material exceeded its initial weight by approximately 0.7% after 22 hours (Figure 3.4). This indicates that the reported silk films can recover after undergoing high temperatures and regain their elasticity. In contrast, silk with 5 wt% $CaCl_2$ exhibited a weight loss of only 3.8% and did not return to its original weight even after 22 hours. These weight fluctuations are attributed to variations in water content, due to presence of Ca^{2+}, which, in turn, have a discernible impact on the modulus of the silk films.

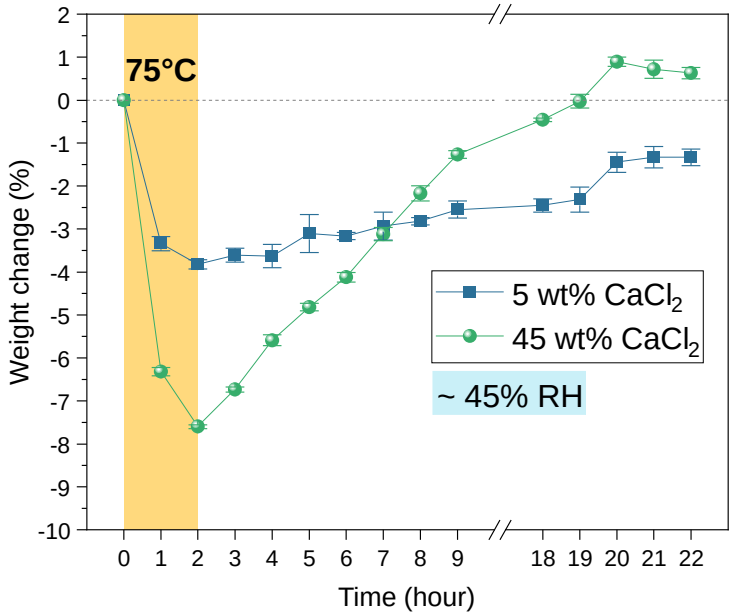

Figure 3.4. The strength of losing and capturing the ambient water molecules of 5 and 45 wt% silk substrates.

3.4.2 Conformality of Silk Substrates on Non-Uniform Surfaces: An Examination of the Interface between Silk and Skin-replica

Figure 3.5a illustrates the elasticity and softness of a 45 wt% $CaCl_2$-loaded red-dyed silk film on a PDMS skin replica. The red-dyed silk films were prepared by incorporating two droplets of a water-based red pigment ink into 20 grams of the pre-formulated silk solution. The PDMS skin-replica was fabricated by mixing Sylgard 184 silicone elastomer (DOW, USA) with its curing agent in a 10:1 ratio. The resulting mixture was stirred for 15 minutes and then poured onto a 60-grit sandpaper. This was followed by a degassing process and a curing period of 2 hours at 75 °C. After solidification in the oven, the interface between the silk and the skin replica demonstrates the tight conformality of the produced silk films in mimicking the surface topography of the epidermis. Indeed, it is essential to have a conformal electrode/skin interface to enhance the stability of the signal recording and reduce motion artifacts, which are the typical limiting factors of the recorded signal-to-noise ratio (SNR) [89]. The surface roughness of the PDMS skin replica is represented with SEM images with an estimated pore size of ~ 180 µm. (Figure 3.5b). the PDMS was carefully detached from the sandpaper and utilized as the skin-replica.

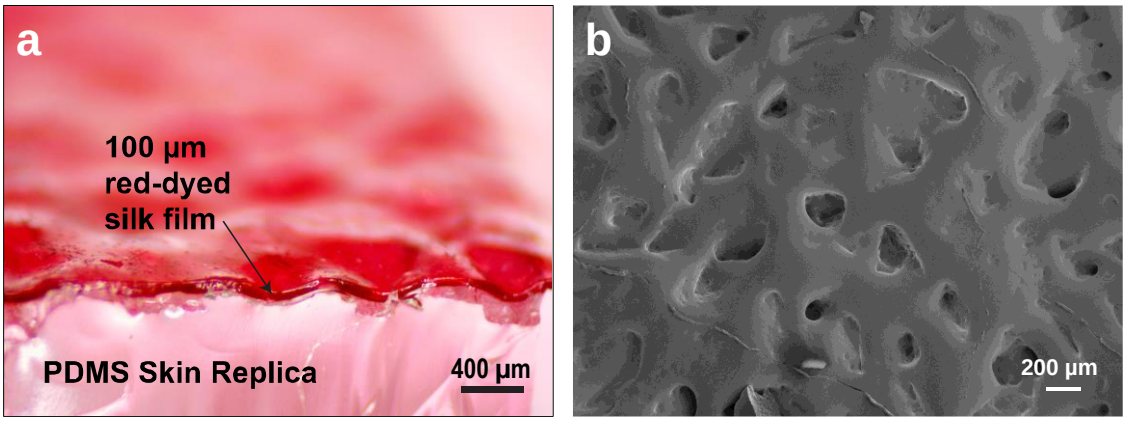

Figure 3.5. Conformality of silk substrate on irregular surfaces. (a) The interface of red-dyed 100 µm silk substrate with PDMS skin replica. (b) Surface topography of PDMS skin-replica. The SEM image represents the surface topology of the prepared PDMS skin-replica, highlighting pore dimensions of approximately 180 µm.

3.4.3 Structural Transition of Silk: From Crystalline β-Sheet Abundance to Amorphous Random Coils

Figure 3.6a presents the characterization of the molecular structures of Ca^{2+}-modified silk substrates, with varying $CaCl_2$/silk ratios, using Fourier-transform infrared (FTIR, Thermo Scientific, Nicolet iS10) spectroscopy. FTIR was employed to characterize the molecular structure of protein-based silk films. The spectroscopic analysis encompassed the wavenumber range from 400 to 4000 cm-1, employing a resolution of 4 cm-1 and each spectrum integrated over 16 scans. In the Amide I region (1600 to 1700 cm^{-1}, C=O stretching group), bands at 1619.91 and 1636.78 cm^{-1} are assigned to the β-sheet and random coil structures, respectively. With the gradual increase in $CaCl_2$ content from 5 wt% to 50 wt%, a noticeable transformation was observed: the β-sheet structures gradually transitioned into random coils. This transformation signifies the shift from a crystalline form to an amorphous one brought about by the interaction of Ca^{2+} ions [90]. Furthermore, the Amide II peak (1500 to 1600 cm^{-1} region, associated with N–H bending groups) displayed a blueshift from 1513 cm^{-1} to 1537 cm^{-1} as the $CaCl_2$ ratio increased from 5 to 50 wt%. These Amide I and II bands are linked to the backbone conformation of the polymer chain and are indicative of the secondary protein structure [91]. Additionally, the Amide A peak (3300 to 3500 cm^{-1} region, corresponding to N-H stretching groups [92]) experienced a redshift, shifting from 3278 cm^{-1} in 5 wt% $CaCl_2$ silk to 3234 cm^{-1} in 50 wt% silk. This shift was attributed to the transition from hydrogen bonding to forming Ca-N bonds through chelate reactions [93], [94]. To further validate this transition from crystalline to amorphous structural alterations, X-ray diffraction (XRD) data (Figure 3.6b) were examined. XRD analysis was executed within the 2θ range of 5° to 54°, employing a scanning rate of 3° per minute with Cu Kα radiation (Bruker D8 Advance instrument, Germany). The parameters were set to an X-ray beam wavelength of 1.5418 Å, a voltage of 40 kV, and a current of 40 mA. The specimens were cut into 1 cm2 squares, each with a uniform thickness of 100 μm, and mounted on the zero-background stand for analysis. The results revealed a broad peak at 26.54° for the 45 wt% compositions, while two peaks were observed at 9.008° and 20.23° in the 2θ scattering angle range for the 5 wt% $CaCl_2$/silk compositions, verifying the transition from crystalline to amorphous structure of the silk protein structures [95], [96].

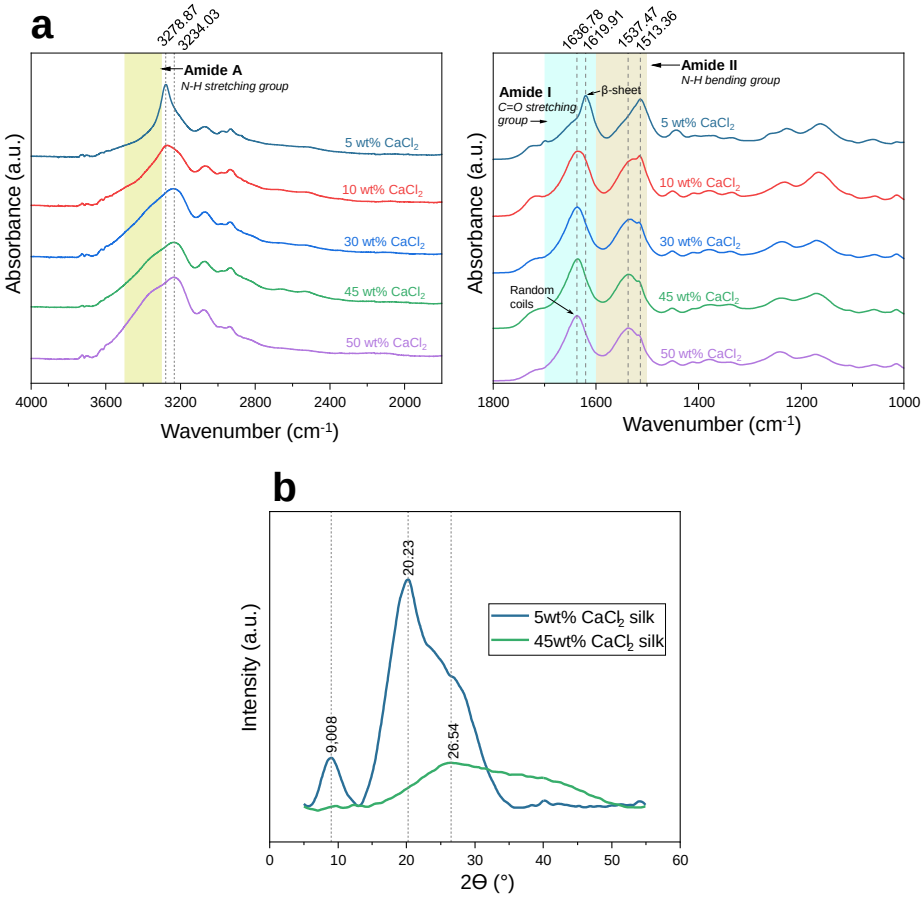

Figure 3.6. Structural transition of silk with varying $CaCl_2$ concentrations. (a) FTIR spectra of different $CaCl_2$/silk ratios illustrate the effect of Ca^{2+} ions on forming beta-sheets and random coils. (b) The X-ray diffraction (XRD) analysis of 5wt% and 45 wt% $CaCl_2$/silk films indicating the transition from a crystalline to an amorphous structure in silk films as the $CaCl_2$/silk concentration increases from 5 wt% to 45 wt%.

3.4.4 Optical Transparency of Silk Substrates

Transparency is a vital biomaterial attribute is which allows epidermal bioelectronics to blend in naturally with the skin tone and reduce their noticeable appearance when worn, where the acceptance and comfort of the user depend on this integration of aesthetics. Figure 3.7 analyzes the transparency of 100 μm silk films with varying $CaCl_2$ ratios. Transmittance measurements of the silk films were conducted using a UV-VIS spectrometer (UV-3150, Shimadzu, Japan) spanning the wavelength range from 400 nm to 2000 nm, using a sample with a thickness of 100 μm. The transmission of these silk

films decreased significantly from an initial level of over 95% to 8% as the $CaCl_2$/silk ratio was reduced from 45 wt% to 5 wt%. This decline in transmission for the silk films with lower $CaCl_2$ loading was attributed to light scattering originating from larger crosslinking sites predominantly consisting of β-sheet structures [97]. Furthermore, the developed silk films exhibited higher transparency than widely-used PET films in wearable devices by approximately 7% [98], [99], [100]. Moreover, in the event of 100% stretching of the 45 wt% $CaCl_2$/silk film, the decrease in transparency of 95 to 78% was negligible.

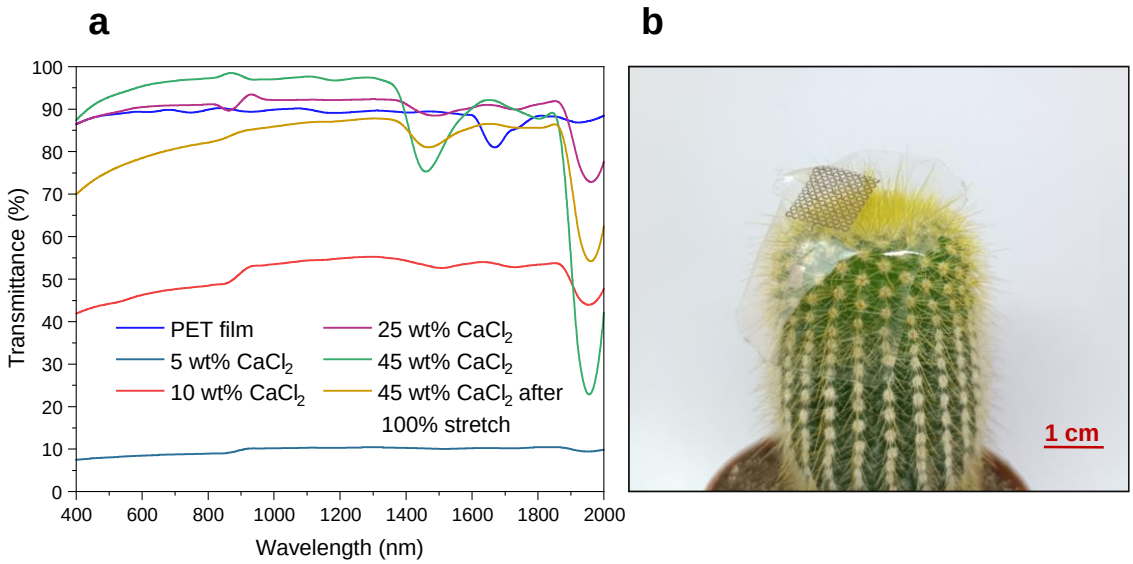

Figure 3.7. Transmittance analysis of the silk substrates with different CaI_2/silk weight ratios.

3.4.5 Adhesion Force and Self-adhesivity of Silk Substrates

Epidermal bioelectronics also require high adhesion and efficient air permeability to maintain stable signal recording, and when worn on the skin for prolonged periods, they should not irritate. As of now, the acquisition of commercial medical-grade adhesives has been instrumental in achieving these properties. However, distinct adhesives tailored to specific applications are necessary for sensitive skins (such as newborn babies or the elderly). Furthermore, despite their effectiveness, the attachment and subsequent peeling off of these adhesives, particularly around hairy regions, result in mild discomfort or pain. On the contrary, the present solution is versatile, as it caters to

individuals with sensitive skin and those without, rendering it to be universally applicable. The self-adhesive property of the silk bioelectronics is demonstrated by quantitatively measuring the peel force with respect to glass (Figure 3.8). A 45 wt% $CaCl_2$/silk solution was poured onto a 1 cm × 15 cm Polyamide film and left overnight to allow for the evaporation of formic acid from the solution. The following day, one end of the Polyamide film, with the silk film on it, was attached to a dry glass surface, and the other end was affixed to the mechanical grip of a mechanical tester (Zwick Z100, Germany). The test was conducted at a speed of 50 mm/min and a relative humidity of 75%. A similar method was employed to measure the adhesion force of Polyamide Kapton tape. The adhesion strength was subsequently calculated by dividing the resultant force by the width of the samplesThe resultant force (~300 N/m) was comparable to commercial polyimide Kapton tape (~150 N/m), medical grade adhesives,[101] and previously reported skin-like electronics [82], [84], [102], [103]. Remarkably, the silk films are not severely prone to dehydration as the adhesion force dropped only by 25% after leaving the silk films in ambient air for one week (Figure 3.8b blue curve).

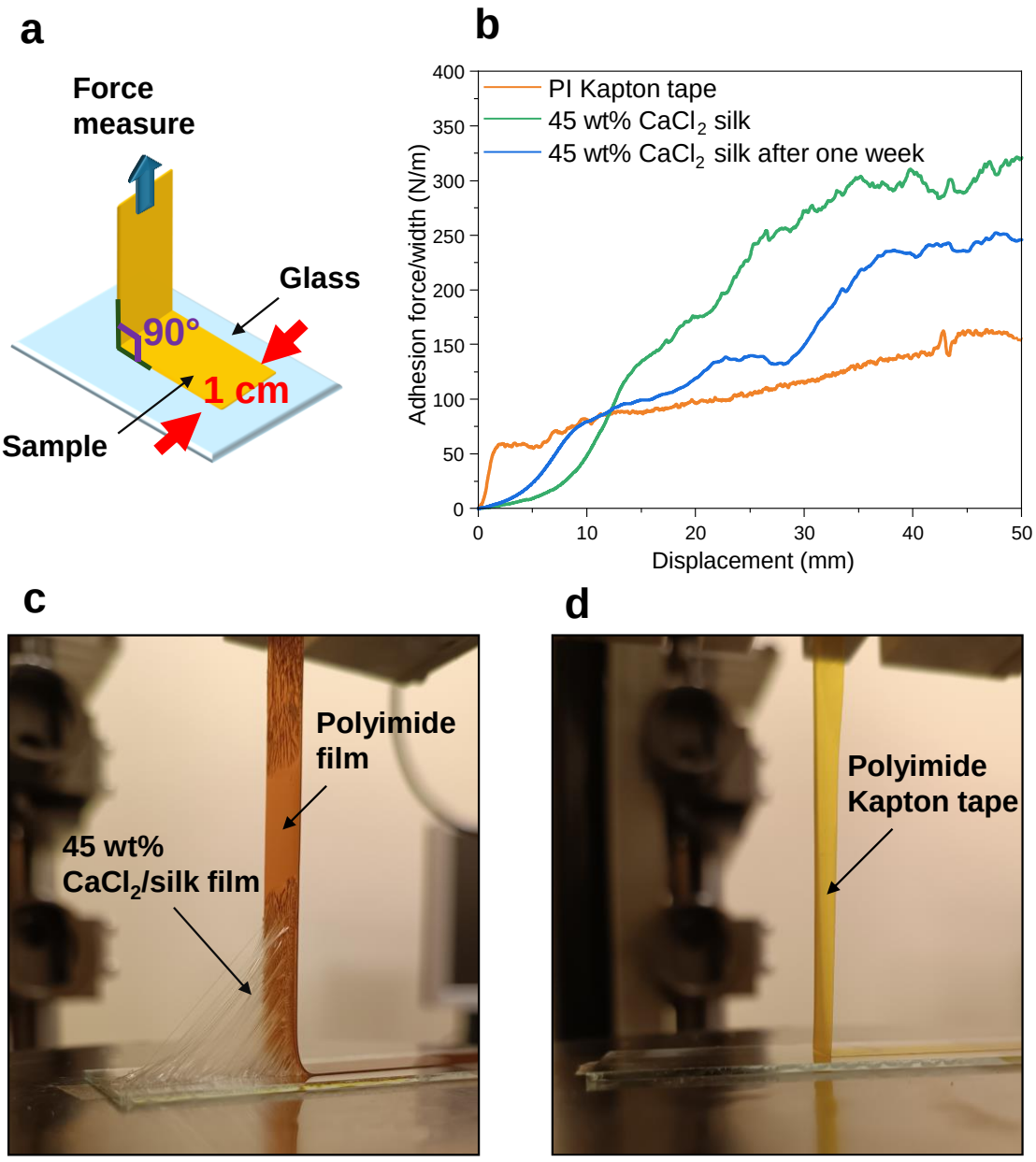

Figure 3.8. Comparative analysis of adhesion force between silk and glass. (a) Schematic of 90° peeling force experiment. (b) Quantitative comparison of adhesion forces between silk substrates and commercial Kapton tape on glass. (c) Adhesion assessment of 45 wt% $CaCl_2$/silk film on polyimide film. (d) Adhesion evaluation of polyimide Kapton tape.

3.4.6 Breathability Analysis

Epidermal bioelectronics should permit the skin-air circulation of water and oxygen to prevent any dermatological infection or allergy (i.e., they should have high air permeability). To show the breathability of the reported silk films, we analyzed the water vapor transmission rate (WVTR) of 45 wt% $CaCl_2$-loaded silk films with a thickness of 100 μm (Figure 3.9)[104]. The WVTR of the silk films was assessed following the ASTM E96-95 standard protocol. A glass vial with a 4 mm opening was filled with 3 mL of distilled water and positioned on an 80 °C hotplate. Subsequently, the vial's opening was sealed with a 100 μm-thick silk film. Then, at regular intervals of 30 minutes over a 3-hour duration, the weight of the vial was measured. The WVTR was then calculated using Equation 1.

$$WVTR = \frac{\Delta m}{t \times A}$$

where Δm is the weight change during t hours, and A is the opening area covered with a sample. Accordingly, the water was heated to 80 °C, and the weight drop due to the evaporated water molecules escaping through the silk films was measured. The obtained WVTR was 1262.6 $g.hour^{-1}.m^{-2}$, which is comparable to that of human skin with a WVTR of ~12 $g.hour^{-1}.m^{-2}$ [105]. To further show the air permeation of the silk substrate *in situ*, thermal analysis was performed after "wearing" the Silk epidermal bioelectronics and commericial gel-based Ag/AgCl electrodes on the forearm for 5 hours, and no temperature variations were observed on the skin region covered with silk epidermal bioelectronics and Ag/AgCl electrodes after immediate thermal imaging (Figure 3.9c-d). These findings highlight Silk epidermal bioelectronics as a promising candidate for an irritation-free electrode, offering extended monitoring periods comparable to those of commercial alternatives.

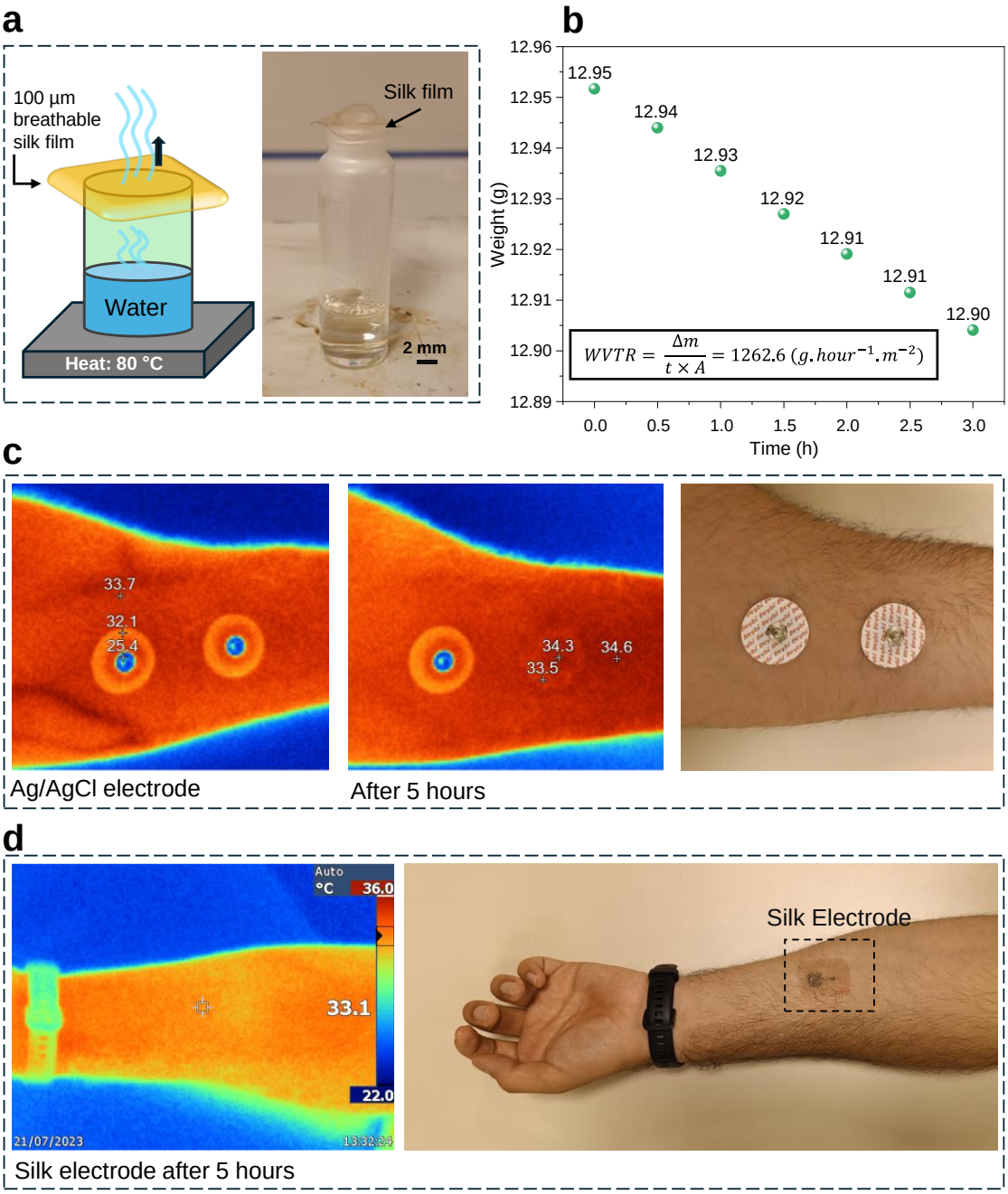

Figure 3.9. Analysis of breathability of silk-based epidermal bioelectronics. (a) Experimental setup for investigating the Water Vapor Transmission Rate (WVTR). (b) Weight variations of a glass vial sealed with a silk film at 30-minute intervals, demonstrating water loss through evaporation via the silk film. The calculated WVTR was found to be 1262.6 $g.hour^{-1}.m^{-2}$. Infrared imaging indicating no discernible temperature variation in skin areas covered by (c) commercial Ag/AgCl electrodes and (d) silk-based epidermal bioelectronics.

3.4.7 Biodegradability Analysis of Silk Films in soil

To investigate the biodegradability of the silk substrates, the films modified with 45 wt% and 5 wt% $CaCl_2$, both with a thickness of 100 μm, were subjected to soil burial and monitored after two days. For the biodegradability test, regular soil rich in organic matter was sieved through a #18 sieve and oven-dried at 60 °C for 4 hours. In each circular plastic container, a total of 25 g of the prepared soil was placed, with the bottom and top diameters of the container measuring 4 and 7 cm, respectively. Following the silk films' placement in the soil's center, the soil was gently moistened once with 4 mL of distilled water. The plastic containers were securely sealed with aluminum foil to maintain appropriate air circulation, allowing for small openings. After an incubation period of 2 days, the soil was sieved once more to assess the silk film degradation rate visually. We show that the 45 wt% silk films achieved complete decomposition in the soil within only 2 days (Figure 3.10). Indeed, this rapid degradation aligns with the FTIR analysis. The prevalence of β-sheet structures in the 5 wt% $CaCl_2$ silk films extended the degradation timeline compared to the 45 wt% $CaCl_2$ silk films, where random coils dominated the structural composition [106]. The remarkable biodegradability exhibited by silk establishes it as an alternative to the commonly used non-biodegradable synthetic polymers for applications in skin-like bioelectronics [26], [29], [107], [108].

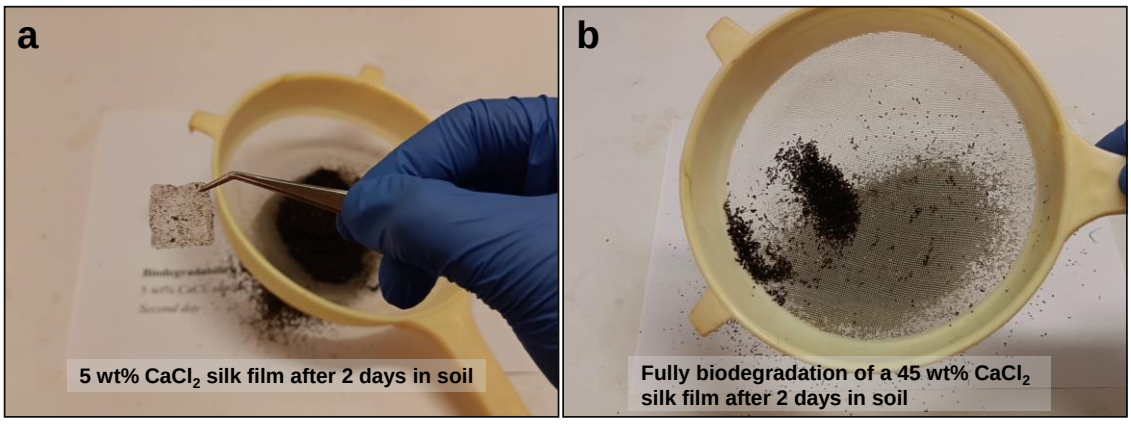

Figure 3.10. Biodegradability analysis of silk films in soil. Two silk films, one with a 5 wt% $CaCl_2$/silk ratio and the other with a 45 wt% $CaCl_2$/silk ratio, both with a thickness of 100 μm, were buried in soil. After a period of 2 days, the soil was sifted to assess the

condition of the silk films. The silk film with a 5 wt% $CaCl_2$ ratio remained intact (a), while the silk film with a 45 wt% $CaCl_2$ ratio was found to be completely degraded (b).

3.4.8 Water Dissolution Rate and Skin Interaction of Silk Films in Aqueous Environments

Any epidermal bioelectronic device may be exposed to high humidity or perspiration and must maintain its structural integrity to ensure optimal performance for long-term monitoring applications (beyond controlled lab conditions). Therefore, water-solubility for the silk films was investigated. A 100 μm-thick, red-dyed silk film containing 45 wt% $CaCl_2$ was subjected to stirring in deionized (DI) water for 5 hours. The silk film did not dissolve during this period (Figure 3.11a). Interestingly, the silk substrates retained their original form and adhesive properties despite being immersed in a water bath (Figure 3.11b). On the other hand, washing off the skin is possible only by gentle rubbing action on the silk patch under water.

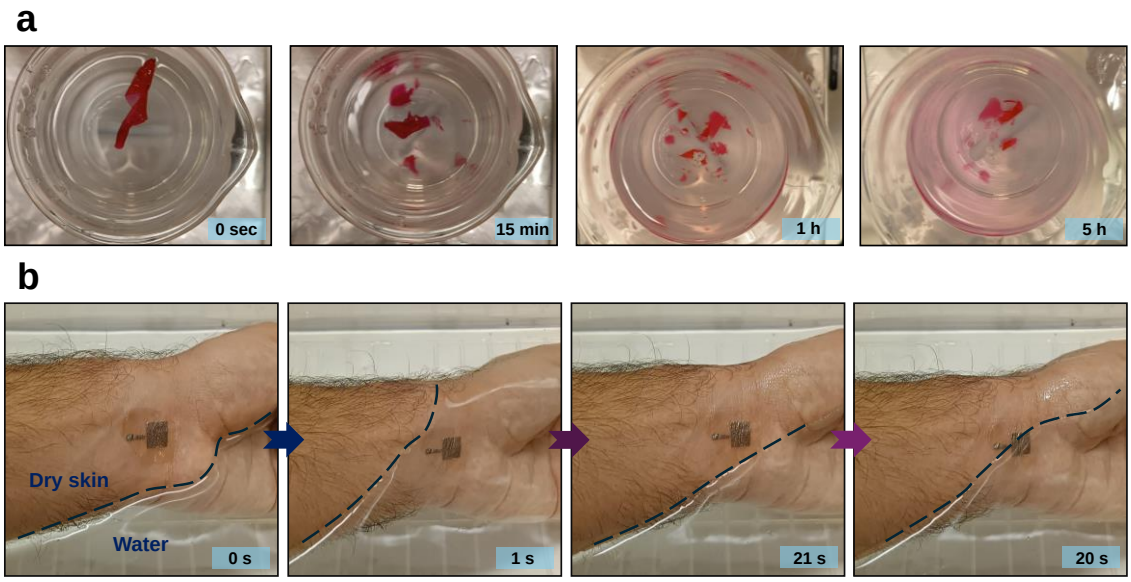

Figure 3.11. Water solubility of silk substrates and their adhesivity performance in aqueous situations. (a) A red-dyed silk film with a 45 wt% $CaCl_2$ ratio and a thickness of 100 μm was submerged in deionized water and subjected to continuous stirring for a duration of 5 hours. The figure shows the film immediately after being placed in the water, after 15 minutes, after 1 hour, and after 5 hours. The results highlight the water-

insolubility of the 45 wt% $CaCl_2$ silk films, suggesting their potential suitability for applications in high humidity or sweat conditions. (b) Evaluation of the adhesion quality of Silk epidermal bioelectronics on skin under water. Prior to submersion in water, during full submersion of the hand in water, with the hand partially submerged and partially exposed to air, and after removal from the water. The observations suggest that complete submersion of the silk-based epidermal electronics on skin in water does not compromise its adhesion quality.

CHAPTER IV

INTEGRATION OF INKJET-PATTERNED SILVER INTO SILK-BASEDEPIDERMAL ORGANIC BIOELECTRONICS WITH FLEXIBLE READOUT CIRCUITRY FOR PHYSIOLOGICAL MONITORING

4.1.Inkjet-printing of Silver Nanoparticle

The Silk epidermal bioelectronics incorporates inkjet-printed serpentine designs featuring a 200 μm trace width, an 800 μm circular diameter, and an overall effective surface area of 1 cm^2 (Figure 4.1a). Achieving high-resolution inkjet printing involved optimizing jetting parameters such as piezoelectric jetting voltage, temperature, and frequency. Figure 4.1b illustrates the jetting profile of 5 out of 12 nozzles. It showcases uniform jetting of AgNP ink droplets from the nozzles, exhibiting perfectly rounded shapes without secondary satellites or stretched filaments. The duration for inkjet-printing a single electrode was estimated to be 5 minutes. The sessile drop method was employed to characterize the PET films' surface-wetting behavior. A liquid droplet (4 pL) was deposited on the substrate and allowed to spread for 10 sec. The side-view profile of the droplet-substrate interface was captured, and the contact angle was measured (Theta Lite optical tensiometer, ON, Canada). The increasing contact angle was regarded as the lower wettability of the substrate. The measured contact angle of 11° between the AgNP ink and the corona-treated donor PET substrate (Figure 4.1c) indicates that the surface energy is sufficiently increased to facilitate the merging of ink droplets on the substrate to form the desired print design. Stylus profilometry indicated a printed AgNP thickness of approximately 500 nm on the donor PET substrate (Figure 4.1d). Following printing, the samples underwent annealing for 20 minutes at an optimized temperature of 140°C. While higher annealing temperatures typically enhance electrical conductivity, the low glass transition temperature of PET substrate at

~78°C restricts higher annealing temperatures due to the risk of physical deformation [109].

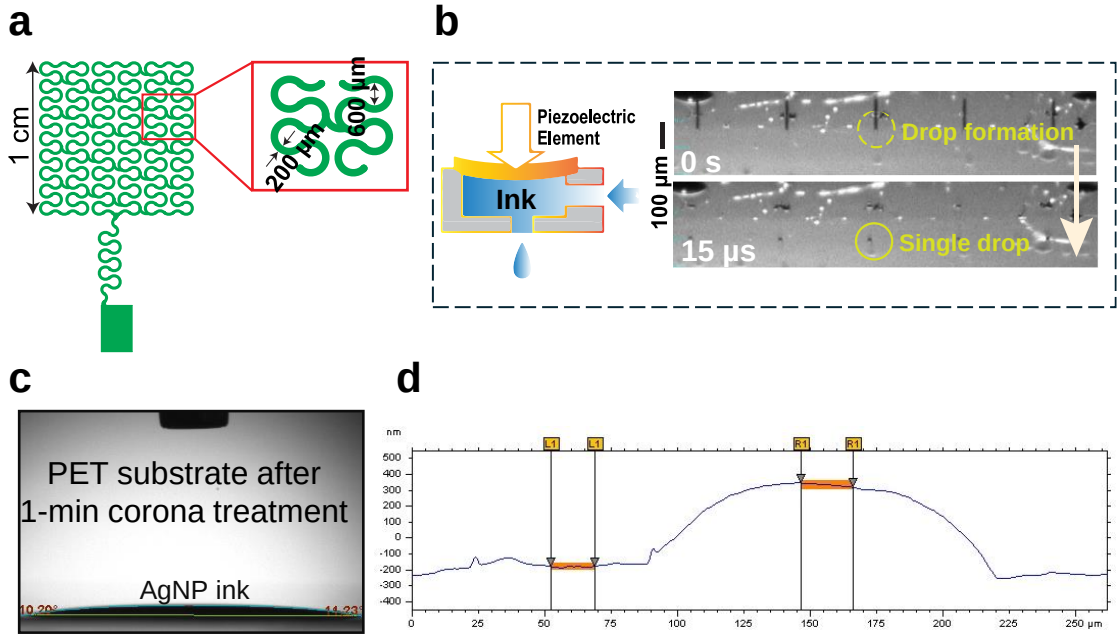

Figure 4.1. Characterizing the inkjet-printing properties of AgNP. (a) Geometry of the serpentine design. (b) AgNP jetting profile of the inkjet-printer head. (c) Contact angle between a PET substrate treated with corona for 1 minute and AgNP ink, with an average value of 10.71°. (d) Profilometer results for a PET substrate with a single cycle of inkjet-printed AgNP. The measured thickness of the printed layer is approximately 514.45 nm.

4.2.Surface Topography of the Inkjet-patterned Silk-based Epidermal Electronics

The surface topography of the patterned silk substrate with AgNP was examined using scanning electron microscopy (SEM, Zeiss Gemini Supra 35 VP, LEO, Germany) operating at an acceleration voltage of 3 kV. To enable the imaging of samples, their surfaces were sputter-coated with a layer of gold-platinum approximately 10 nm thick. The atomic force microscopy (AFM) was assessed using an atomic force microscope (Nanomagnetics Instruments, hpAFM, UK) in tapping mode. The SEM images depict the serpentine pattern of inkjet-patterned AgNP on the silk substrate (Figure 4.2b), with

the printed AgNP estimated to have a nanoparticle size of approximately 75 nm (Figure 4.2c). Furthermore, Figure 4.2a in the SEM image illustrates the surface roughness of the silk electrodes. This observed roughness was compared with the AFM images (Figure 4.2d-e), revealing a maximum surface roughness of 26.29 nm.

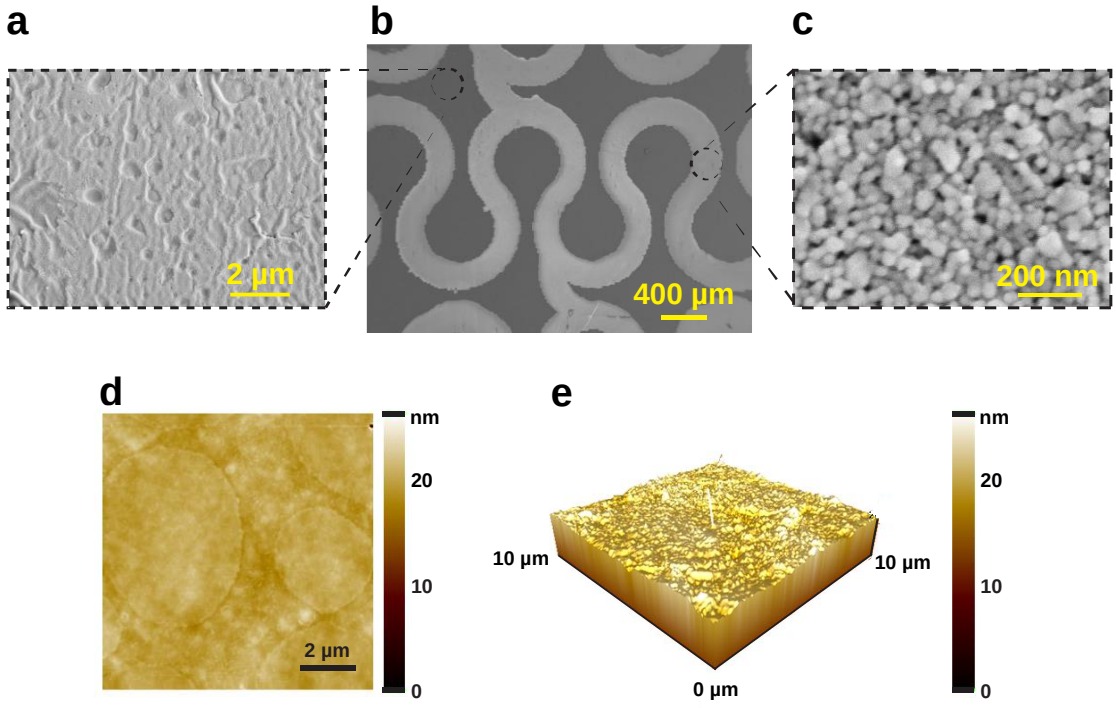

Figure 4.2. Surface topography of the skin-like silk bioelectronics (Silk epidermal bioelectronics). SEM images of (a) the pristine silk substrate section of the Silk epidermal bioelectronics, (b) AgNP patterned Silk epidermal bioelectronics, and (c) Inkjet-printed AgNP section of the Silk epidermal bioelectronics. AFM images showing: (d) the surface topology, and (e) 3D topography of the silk substrate.

4.3. Susceptibility of the Printed AgNP Patterns to Oxidation: Shelf time Investigation

Patterns are susceptible to oxidation due to ambient air which potentially impacts their mechanical and electrical properties. To demonstrate the shelf-life of inkjet-printed

silver-based soft electronics, we conducted experiments revealing that low humidity conditions can effectively safeguard the AgNP electrodes from oxidation (Figure 4.3). Samples stored in a desiccator exhibited no signs of oxidation or changes in resistance compared to those exposed to ambient air, which displayed a resistance increase of 76.3% after 1 month. Despite the large percent change in resistance, the initial resistance of the printed structures (4.65 Ω) only changes by ~3.55 Ω in 1 month, bringing the final resistance to 8.2 Ω which is still very conductive for a typical single-use biopotential electrode. Therefore, we envision that inkjet-printed, silver-based soft electronics can still be re-used for durations in excess of a couple of months for various applications including human vital signs monitoring.

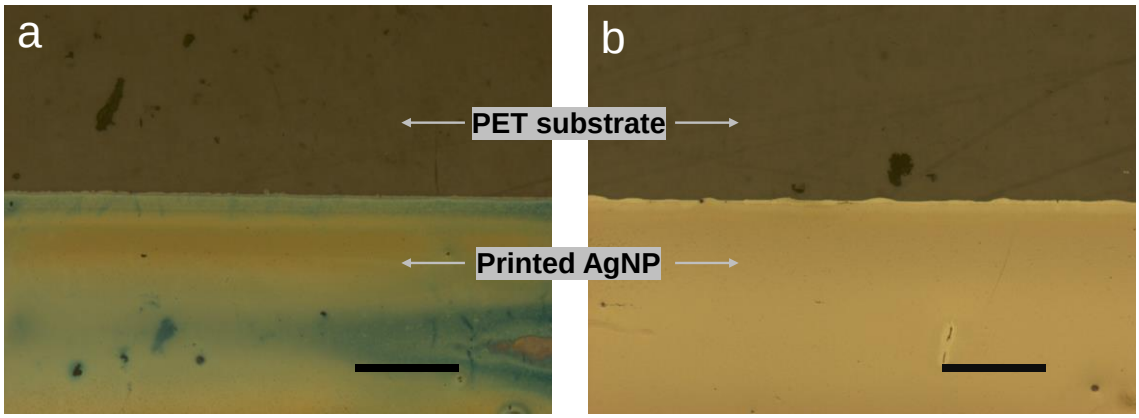

Figure 4.3. Impact of ambient air on the oxidation of inkjet-printed AgNP samples. a) Microscopic image of inkjet-printed AgNP ink on a PET substrate that was left in ambient air for 1 month. The sample underwent oxidation, and its resistance varied from 4.65 to 8.2 Ω. b) Microscopic image of inkjet-printed AgNP ink on a PET substrate that was preserved in a vacuum desiccator. The sample did not oxidize, and its resistance remained stable. These results suggest that samples patterned with AgNP have a long shelf-life under low humidity conditions. Scale bar, 400 µm.

4.4. Skin Conformality and Electrical Performance of Inkjet-patterned Silk-based Epidermal Electronics

Conformal attachment of Silk epidermal bioelectronics in mimicking the skin deformations under stretching, compressing, and twisting is shown in Figure 4.4a. To assess the resistance changes in the silk electrodes during elongation, a 20% strain was applied to the samples using a precision brushed motor (Thorlabs, MTS50A-Z8, USA) with an operating speed of 6 mm/min. Resistance measurements were obtained utilizing a precision benchtop multimeter (GDM-9061, GW Instek, Taiwan). When subjected to a 20% strain, the recorded electrical resistance exhibited a maximum change of 352.5 kΩ (Figure 4.4b). This change in resistance is attributed to surface cracks in the printed AgNP that emerge under strain. The increased resistance gradually returns to its initial value once the strain is removed, primarily because the transition from plastic to elastic deformation in the silk substrate occurs gradually.

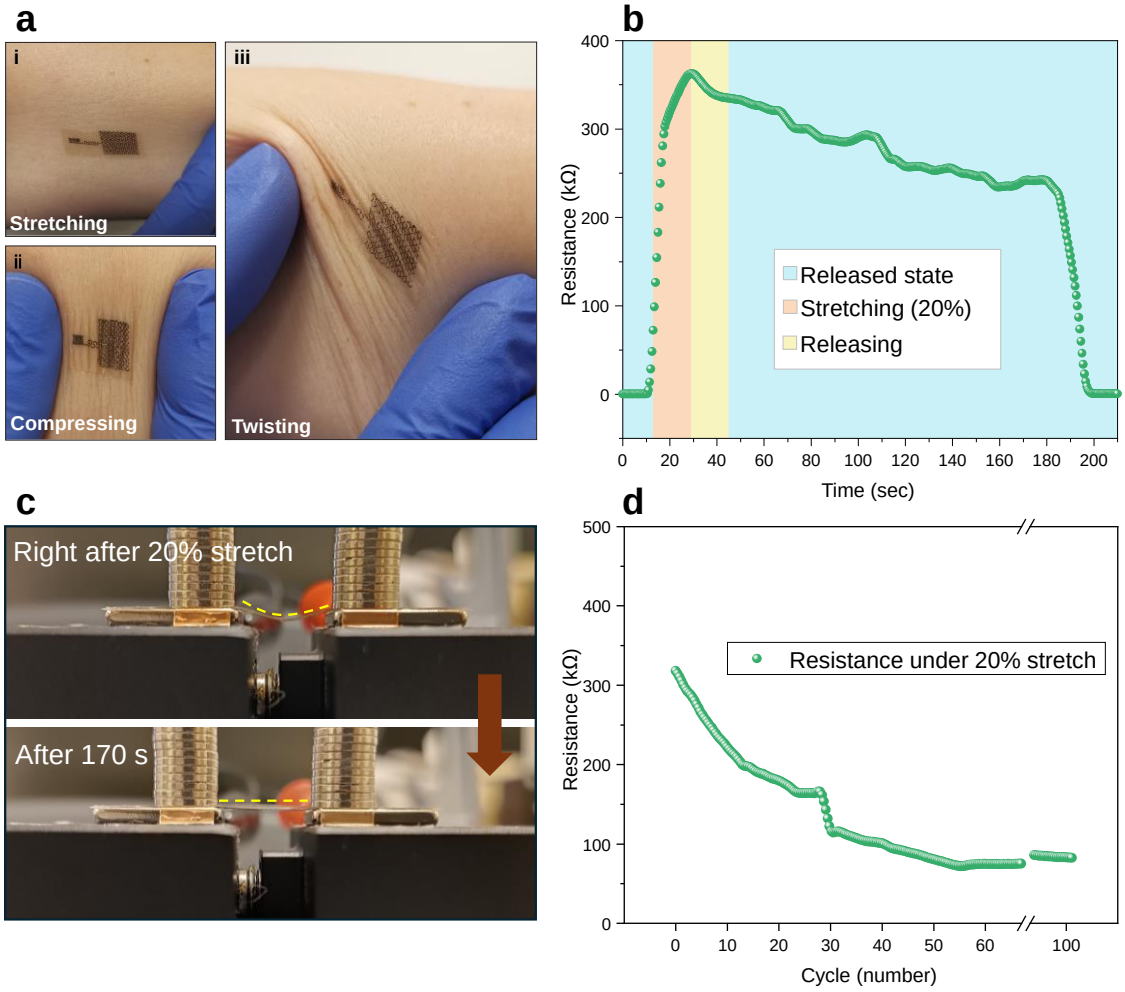

Figure 4.4. Characterizing the skin conformality and electrical performance of inkjet-patterned silk-based epidermal electronics. (a) Silk epidermal bioelectronics on the skin under (i) stretching, (ii) compressing, and (iii) twisting motions. (b) Resistance variation

of the patch under 20% stretching and releasing tests. (c) Plastic deformation of silk right after 20% stretch-release to initial form ater 170 seconds. (d) Resistance variation profile of the patch in 100 times cyclic stretching-releasing.

The electrical performance of the Silk epidermal bioelectronics was further evaluated by attaching an electrode integrated with a light-emitting diode (LED) to a balloon (Figure 4.5a). A consistent electrical connection maintained the illumination of the LED as the Silk epidermal bioelectronics underwent stretching or compression with the inflation or deflation of the balloon. Similarly, the electrode with an LED exhibited stable performance on the skin during stretching, twisting, and compressing (Figure 4.5b). The durability/endurance of the Silk epidermal bioelectronics was also assessed through cyclic of stretching and releasing at 20% strain for 100 repetitins. Throughout these cycles, the electrode resistance decreased from approximately 300 to about 80 kΩ when subjected to 20% stretch.

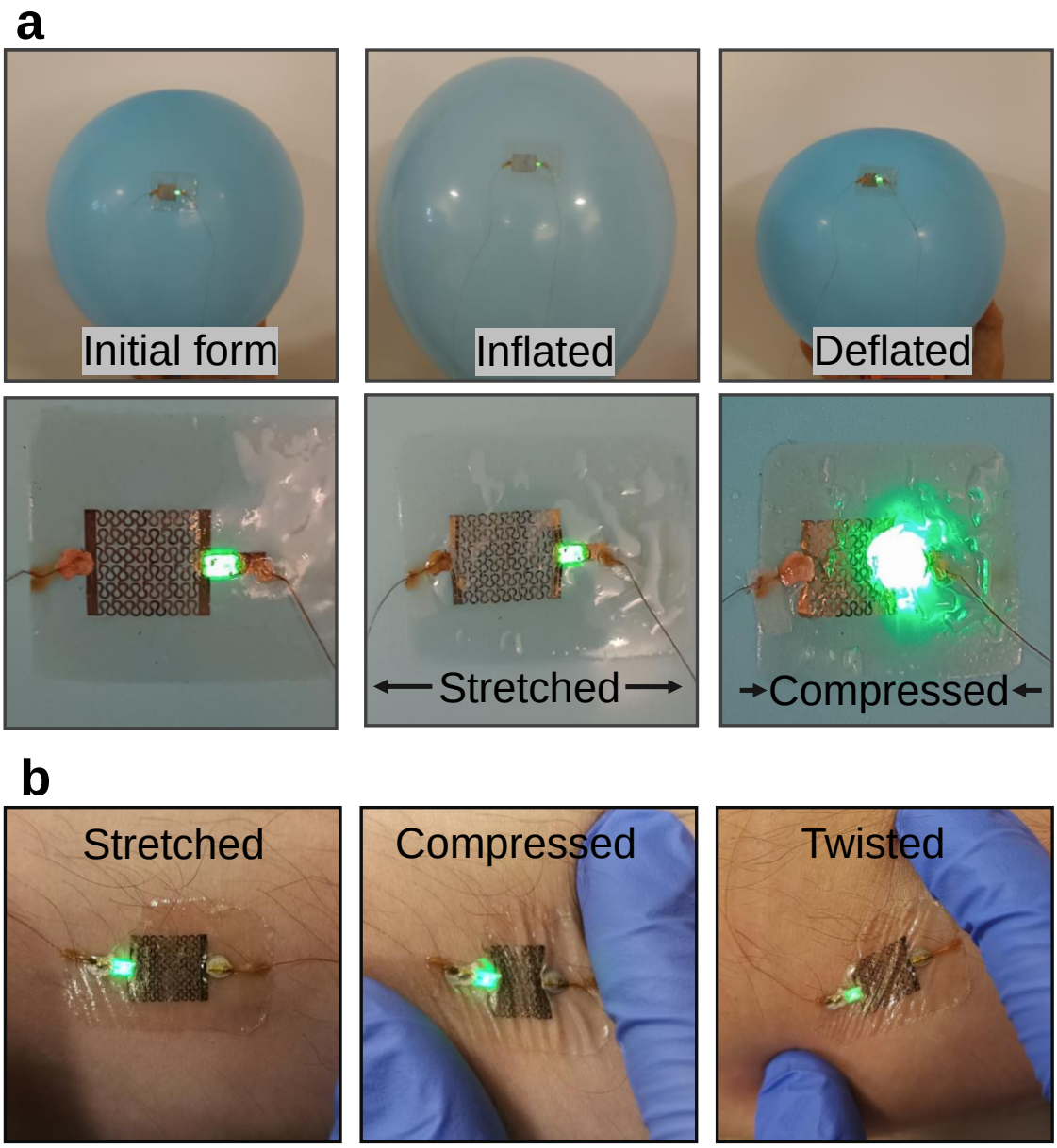

Figure 4.5. Electrical performance of silk-based epidermal electronics under various deformations. (a) The images depict an LED-integrated Silk epidermal bioelectronics attached to a balloon. (a) Silk epidermal bioelectronics after attachment to the balloon. (b) Silk epidermal bioelectronics stretched over the inflated balloon. (c) Silk epidermal bioelectronics in a compressed state after the balloon has been deflated, relatively to its initial form. The results demonstrate that the Silk epidermal bioelectronics maintains its electrical conductivity regardless of whether the balloon is inflated or deflated. The deformations experienced by the balloon can be likened to natural skin deformations, which involve stretching and compression. (b) Electrical performance of an LED-integrated silk electrode applied to skin under various skin deformations. The findings

reveal that the Silk epidermal bioelectronics maintains stable electrical conductivity, even when subjected to natural skin deformations.

4.5. Development of a Flexible, Wireless Electronic Circuit for Integration into Silk-Based Epidermal Electronics

The integration of Silk epidermal bioelectronics with our flexible readout circuitry having a 15 mm × 70 mm footprint forms a compact system capable of continuously recording various electrophysiological biosignals, such as non-invasive biopotentials. The schematic and printed circuit board (PCB) design for the biopotential unit were designed using Altium Designer 22.2.1, and the flexible board was manufactured commercially. The soldering process involved the application of solder paste (OM-5002, Alpha) to the flexible board using a stencil. Subsequently, the electrical components were positioned on the board. The board was then heated at 220°C for 5 minutes, which melted the solder paste and secured the components to the board. The flexible signal acquisition unit was attached on skin using double-sided silicone/acrylate thermoplastic elastomer medical tape (2477P), purchased from 3M (USA).The sensing circuitry (Figure 4f) comprises an instrumentation amplifier (INA) with a gain of 180, followed by a low-pass active filter (LPF) set at a 1 kHz cut-off frequency without gain. The analog signal then enters a 32-bit resolution delta-sigma analog-to-digital converter (ADC) operating at a sampling rate of 360 samples per second for further processing. Power is supplied by a rechargeable 12 mAh lithium-ion battery, managed by the battery management unit for on-board recharging. A Bluetooth low energy (BLE) system-on-chip (SoC) facilitates the reception of digitized data from the ADC and its wireless transmission to a nearby smartphone. The individual components of the readout circuit were assembled on a flexible printed circuit board (FPCB), which can bend and conform to various curved surfaces for seamless integration into the human body and the wearable Silk epidermal bioelectronics. The electrical performance of the flexible device remains consistent even under mechanical bendings exceeding 90°, surpassing the natural deformations of the body regions of interest, such as the chest, neck, and forearm.

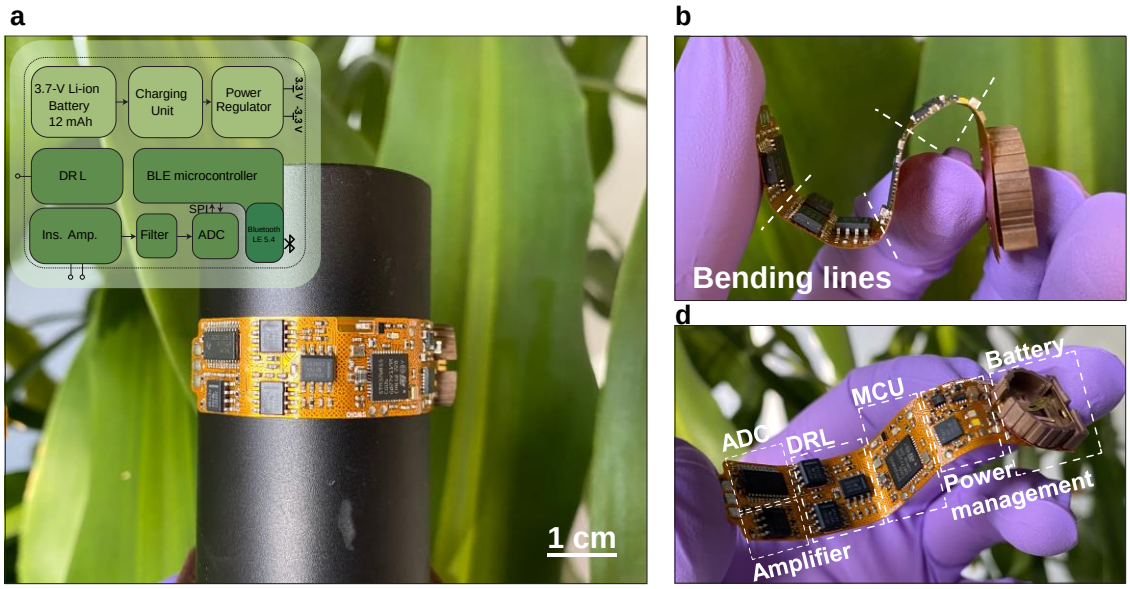

Figure 4.6. Flexible and wireless readout circuitry. The figure demonstrates Flexible circuitry (a) on a curved surface with an inset block diagram of the different parts of the circuitry., (b) folded by hand, and (c) bent in hand and illustrating the different parts of the system. DRL: driven right leg. BLE: Bluetooth low energy. Ins. Amp.: instrumentation amplifier. ADC: analog to digital converter. SPI: serial peripheral interface.

CHAPTER V

ELECTROPHYSIOLOGICAL SIGNAL RECORDING USING SILK-BASED INKJET-PATTERNED EPIDERMAL ORGANIC BIOELECTRONICS

5.1. Cardiovascular Evaluation Using Electrocardiography (ECG)

The Silk epidermal bioelectronics can capture electrical biopotential signals throughout human skin emanating from physiological processes. For the collected biopotential signals, offline processing was carried out in MATLAB. The initial step involved the removal of signal baselines. Subsequently, a notch filter with a quality factor of 35 was applied to eliminate the 50 Hz powerline noise. Depending on the type of signal collected, a band-pass filter specific to that signal type was employed. Finally, a moving average filter was applied to further enhance the signal quality. To demonstrate its functionality, we collected ECG signals in a standard lead-I configuration by placing the Silk epidermal bioelectronics on the left and right inner wrist as differential electrodes while the ground electrode was positioned on the left arm (Figure 5.1a). These electrodes, characterized by their high elasticity, proved ideal for acquiring high-quality ECG signals showcasing distinguishable P-QRS-T segments (Figure 5.1b-c). The fidelity of these signals allows for diagnosing cardiovascular conditions like ischemic heart disease and myocardial infarction [110] and estimating heart rate in real-time. The peak-to-peak voltage of the recorded ECG signals measured approximately 60 mV, with the gain of the flexible electronic circuitry set at 180, and the Welch spectral density estimation indicates a power value of 33 dB for the R-peak within the frequency range of 0-150 Hz (Figure 5.1d).

The superior self-adhesiveness of the silk electronics ensures a conformal attachment to the skin, enabling the recording of ECG signals for up to 12 hours without any compromise in signal quality. Throughout this duration, the participant was able to engage in routine activities such as sleeping, eating, and performing physical tasks like laboratory work. To ensure the accuracy of the ECG recordings and verify that the adhesivity of the silk had not degraded during the 12 hours, ECG signals were recorded at one-hour intervals in a stationary position. Figure 5.1f presents the 5-second snapshots of these recordings, providing a total of 12 distinct ECG signals over the 12-hour period.. The RMS noise values fluctuated between 50 and 82 μV, with an average value of 66.5 μV. This highlights the minimal influence of body movements on the adhesiveness of the Silk epidermal bioelectronics, thereby affirming the consistent performance of the electrode.

Interestingly, the self-adhesive Silk epidermal bioelectronics exhibits even lower skin-electrode impedance than commercial electrodes equipped with adhesive backing within the 10-1000 Hz range (Figure 5.1g). The skin and electrode interface impedance was investigated using an LCR meter (GW Instek, LCR-6002, Taiwan). The skin was cleaned and dried prior to the experiment. The silk skin electrodes as the measuring electrode and commercial “wet” silver/silver chloride (Ag/AgCl) electrodes (Beybi, China) were placed as the reference electrode with 5 cm spacing on the forearm of the volunteer. The impedance changes were recorded between 10-1000 Hz [111]. Impedance measurements at 10 Hz showed values of 450.67 kΩ for the Ag/AgCl electrodes and 337.16 kΩ for the Silk epidermal bioelectronics. The decreased impedance of the Silk epidermal bioelectronics is attributed to its exceptional elasticity and robust adhesion at the interface between silk and skin. These material properties facilitate minimal air gaps between the skin and the electrode, reducing the capacitive effect and consequently lowering impedance values [89].

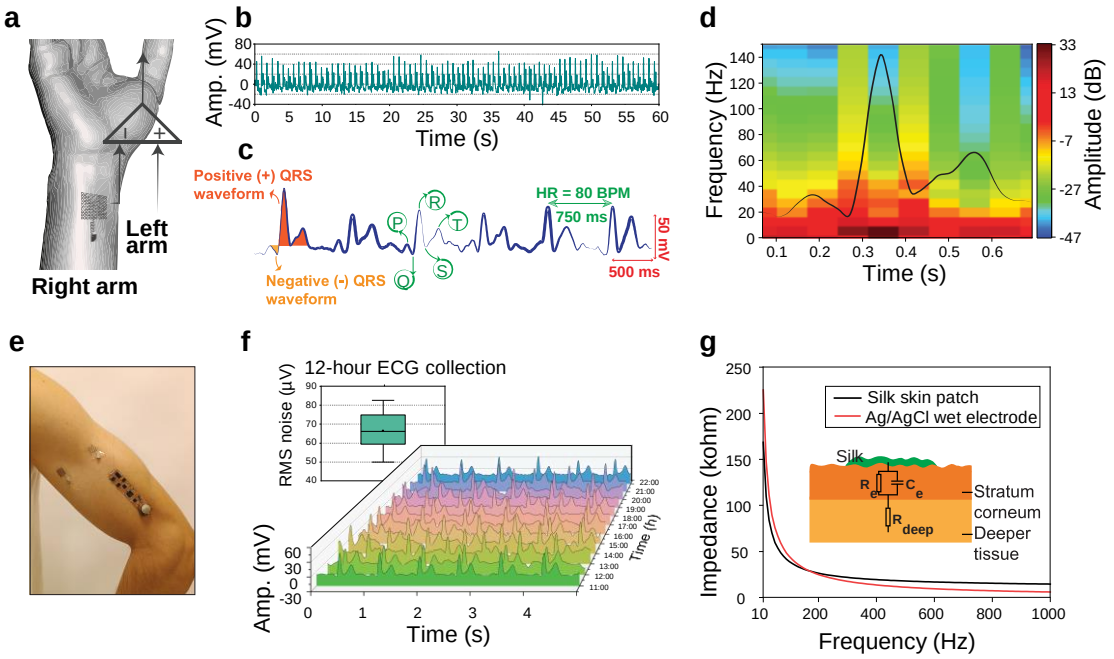

Figure 5.1. Electrocardiography (ECG) monitoring using silk-based epidermal biolectronics. (a) ECG signal collection using skin-like silk bioelectronics. (b) P-QRS-T complex identification with an estimated heart rate from the recorded ECG signal. (c) Power analysis of the recorded ECG signal. (d) Schematic illustration of the Silk epidermal bioelectronics placement for ECG recording. (e) Silk epidermal bioelectronics integrated with the flexible signal acquisition unit. (f) Extended ECG monitoring using the Silk epidermal bioelectronics over 12 hours. (g) Comparison of skin-electrode impedance between "soft" Silk epidermal bioelectronics and commercial "wet" Ag/AgCl electrodes where the inset shows an illustrative electrical model of the impedance.

Furthermore, a comparative assessment was conducted to evaluate the performance of our "soft" silk electrodes in parallel with commercial "wet" Ag/AgCl electrodes for simultaneous ECG signal measurement using a commercial open-source Open-BCI data acquisition unit (Figure 5.2). The recorded signals from both the Silk epidermal bioelectronics and Ag/AgCl electrodes exhibited an almost excellent Pearson's correlation ratio of 99.4% and similar signal-to-noise ratio (SNR) values of 9.09 dB (Silk epidermal bioelectronics) and 10.08 dB (Ag/AgCl), affirming the high fidelity of the Silk epidermal bioelectronics in capturing ECG signals.

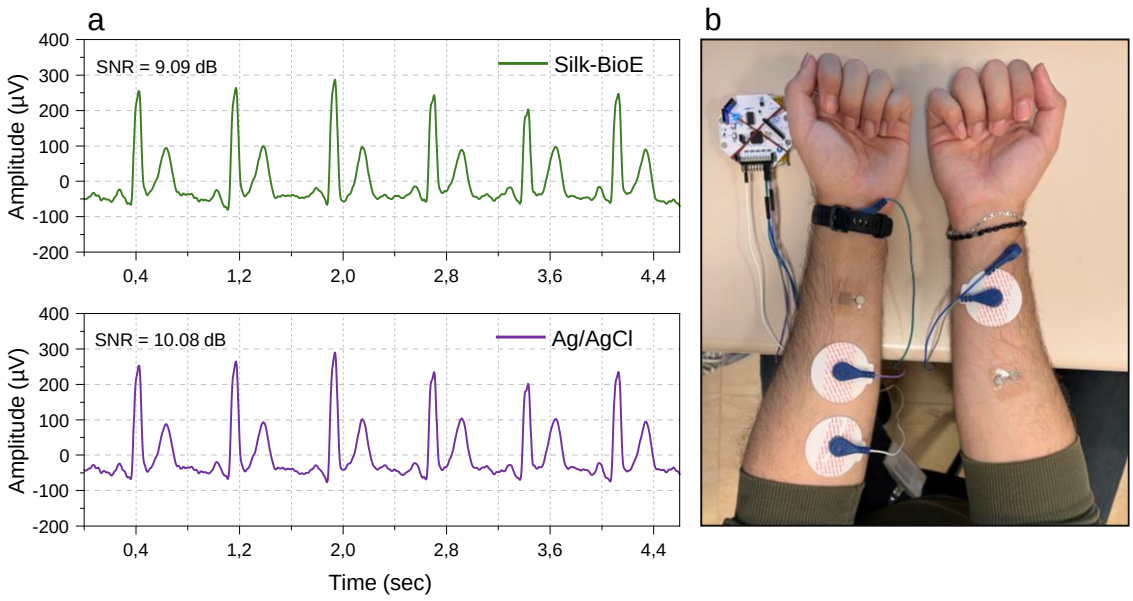

Figure 5.2. Simultaneous ecg recording using silk epidermal bioelectronics and Ag/AgCl electrodes. a) The recorded ECG signals exhibit SNR values of 9.09 dB for Silk epidermal bioelectronics and 10.08 dB for Ag/AgCl, respectively. These signals demonstrate a Pearson's correlation coefficient of 99.4%. b) The figure illustrates the setup for ECG collection in a lead-I configuration, along with a commercial signal acquisition board (Cyton board, OpenBCI).

5.2.Electromyography (EMG) and its Application in Wearable Fitness Monitoring

The unique properties of the Silk epidermal bioelectronics, including self-adhesiveness, stretchability, and breathability, render it exceptionally suitable for assessing the electrical activity of the bicep brachii through recording electromyography (EMG) signals. EMG signal collection typically targets specific muscle groups during consistent physical activity, which can induce considerable skin deformation and motion artifacts. Choosing an inappropriate electrode under such conditions may compromise signal quality and data loss. Self-adhesive and stretchable electrodes prove advantageous for EMG signal recording as they mimic severe skin deformations and enhance signal fidelity. Additionally, the skin's increased sweat production during physical activity necessitates breathable materials to prevent potential localized skin trauma [112]. To record EMG signals, a pair of Silk epidermal bioelectronics electrodes

were positioned 2 cm apart on the right bicep (Figure 5.3a). The participant performed a series of exercises involving lifting dumbbells of varying weights and maintaining muscle contraction for 10 seconds, followed by a 10-second relaxation period. This experiment was repeated using dumbbells weighing 4, 6, and 8 kg. The recorded EMG signal amplitudes during muscle contraction were approximately 10, 20, and 30 mV for the 4, 6, and 8 kg weights, respectively (Figure 5.3b). Furthermore, the intensity of the measured signal demonstrated a linear correlation with the dumbbell weight, exhibiting a Pearson correlation coefficient (r) value of 0.99 (Figure 5.3c).

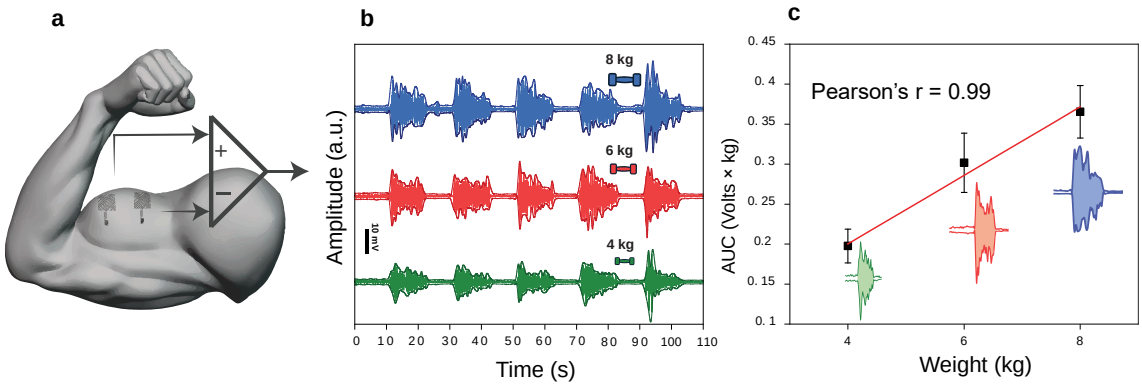

Figure 5.3. Electromyography using silk-based epidermal bioelectronics for fitness applications. (a) The placement of Silk epidermal bioelectronics electrodes on the bicep for EMG monitoring. (b) EMG signals were recorded in real time during the contraction and relaxation phases of the bicep muscle in lifting various dumbbells. (c) Calibration curve linking the area under the curve (AUC) of EMG signals to the weight of different dumbbell weights, which can be used to quantify exercise intensity in training or in notifying/predicting muscle fatigue.

5.3.Electrooculography (EOG) in Characterizing Eye Movement

Furthermore, the application of Silk epidermal bioelectronics extends to collecting electrooculography (EOG) signals. In our setup, differential electrodes were positioned on the right and left temples (Figure 5.4a), and as the participant shifted their gaze between right and left orientations, a distinct alteration in voltage amplitude in the cornea-retinal potential, spanning from the front to the back of the eye, was observed.

This particular change bears significance in identifying ocular disorders, facilitating early diagnosis of macular degeneration, and fostering advancements in human-computer interaction (HCI) [113], [114]. The recordings illustrated in Figure 5.4b depict the EOG signals acquired through Silk epidermal bioelectronics and flexible circuitry while the participant executed swift horizontal eye movements at regular intervals. The experimental protocol involved the participant looking forward, then shifting their gaze successively to the left, returning to the center, and subsequently to the right, each position held for 10 seconds. The distinctive signal profiles during left and right eye movements exhibited fluctuations within the approximate range of -30 to 30 mV. Analysis using Welch's Fourier transform unveiled power magnitudes in the recorded signals oscillating between -110 and 30 dB (Figure 5.4c).

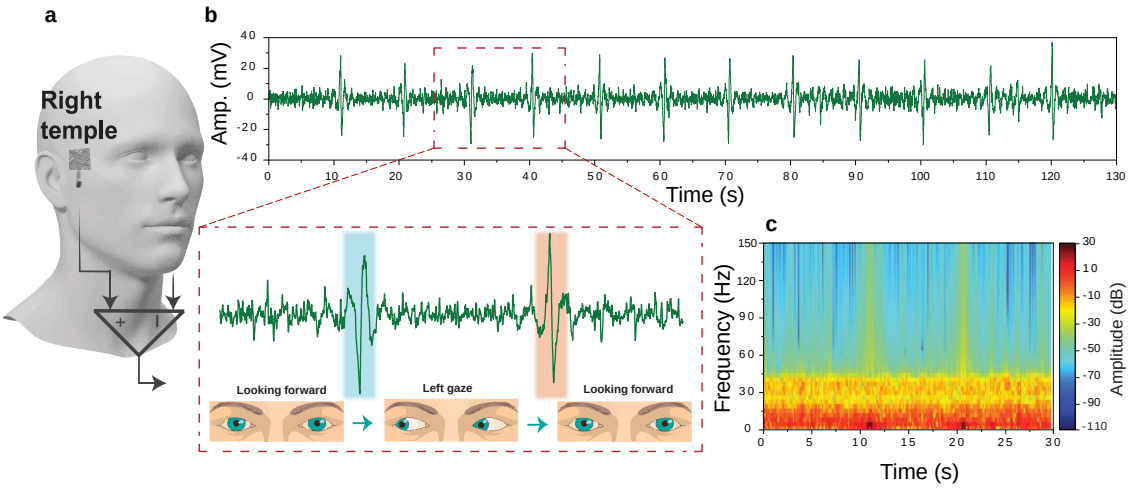

Figure 5.4. Electroculography for the characterization of eyeball movement. Electrode placement for eog recording. (e) EOG acquisition by Silk epidermal bioelectronics during left and right eye rotations can be used within activity recognition and mobile human-machine interaction (HMI). (f) Analysis of the EOG power spectrum density.

5.4.Electroencephalography (EEG) for the Detailed Characterization of Neural Activity Patterns

We investigated single-channel EEG signal recording with the Silk epidermal bioelectronics. Electrodes were positioned in a configuration adhering to the universally

standardized 10-20 system, specifically on Fp1 and A1 (Figure 7a). While all the previous biopotentials (ECG, EMG, and EOG) typically exhibit voltage amplitudes in the milli-volt range, EEG signals fall within the micro-volt range, rendering them particularly susceptible to noise. Therefore, the performance of both electrodes and the electronic signal acquisition unit is critical in meeting the stringent requirements for EEG signal collection. To validate the accuracy of the recorded EEG signal, we assessed the generation of alpha-band frequencies. The alpha band, spanning from 8 Hz to 12 Hz,[115] typically manifests during participant relaxation, particularly when their eyes are closed. As such, the participant was instructed to open and close their eyes every minute alternately. Time-domain EEG signals recorded using Silk epidermal bioelectronics and the flexible signal acquisition unit are depicted in Figure 7b. In part i of Figure 7b, the EEG signals manifest distinct sharp spikes associated with voluntary eye blinks (EOG), marked by an approximate amplitude of 400 μV. However, during the eye closure, these spikes are substituted by the rapid eye movement state (REM). Higher-frequency alpha-band generation is also discernible in the time-domain results (Figure 7b ii, iii). On the other hand, the interesting observation of the presence of ECG (R-peak) within the recorded EEG signals underscores the high performance of Silk epidermal bioelectronics in capturing high-resolution biosignals and low-noise recording where even the forehead ECG signals are distinguished. Indeed, the short-time Fourier transform (STFT) illustrates the occurrence of alpha-band frequencies (7-11 Hz) when eyes are closed (Figure 7d). Furthermore, Welch's Fourier transform analysis depicts a power magnitude of 80 dB within the recorded EEG signals.

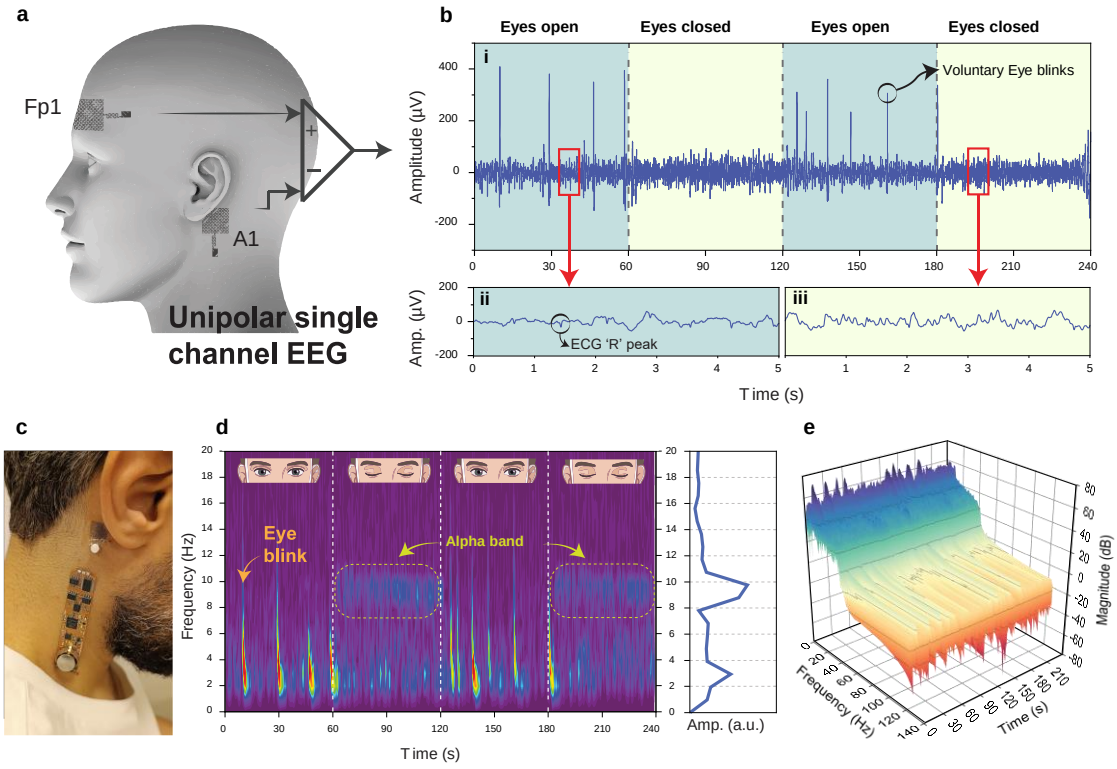

Figure 5.5. EEG signal acquisition using silk epidermal bioelectronics: (a) schematic representation illustrating the placement of silk epidermal bioelectronics electrodes on fp1 and a1 for EEG acquisition. (b) Time-domain EEG signals were captured during both the open and closed-eye states of the participant. Insets emphasize frequency variations observed during the alternating eye movements. (c) Integration depiction of Silk epidermal bioelectronics with the flexible signal acquisition board for EEG signal collection. (d) Frequency-domain representation of EEG signals highlighting the emergence of alpha-wave frequencies during closed-eye states. (e) Power spectrogram showcasing the spectral analysis of the EEG recordings.

To further evaluate the performance of the proposed Silk epidermal bioelectronics and electronic circuitry in EEG signal recording, participants were tasked with maintaining relaxed open-eye states for 60 seconds, followed by closing their eyes and engaging in focused mental arithmetic exercises with intense concentration (e.g., such as calculating the product of 12 to 135). Results reveal the emergence of beta frequencies (15 - 18 Hz) during focused closed-eye states (Figure 5.6).

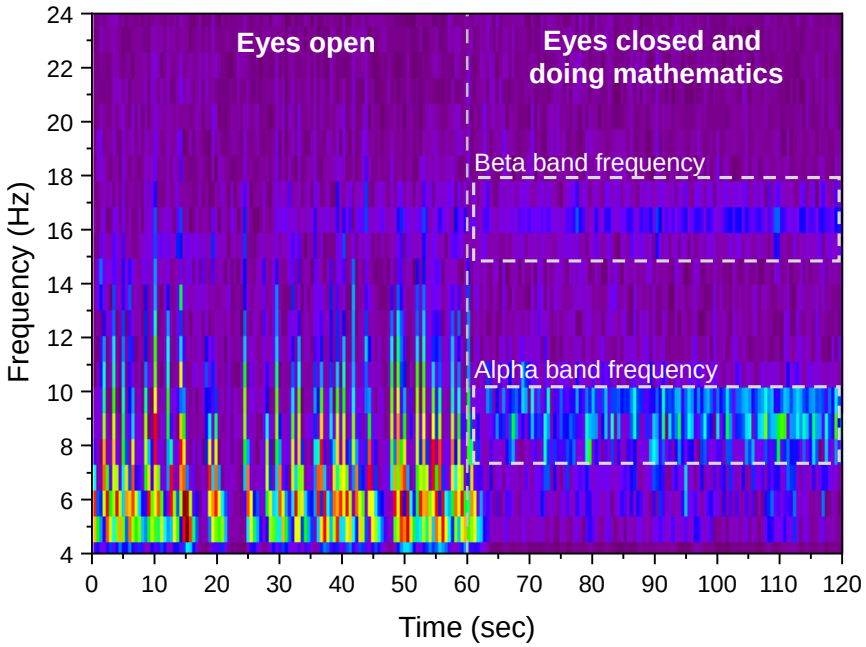

Figure 5.6. Fast Fourier transform spectroscopy of EEG signals recorded using silk epidermal bioelectronics, aimed at investigating beta-band frequencies during deep meditation phases. The participant was instructed to keep their eyes open and gaze forward for 60 seconds, followed by closing their eyes and performing basic mathematics for another 60 seconds. The results indicate that this sequence induced the generation of alpha bands due to eye closure, and beta bands due to the mental activity involved in performing mathematical tasks.

CHAPTER VI

CONCLUSION

This study introduces a tailored solution for epidermal bioelectronics by unifying all the essential features that skin-interfaced “skin-electronics” must possess, and do so by reformulating of the green synthesis of an ancient material—protein-based natural silk derived from *bombyx mori* cocoons. Departing from the conventional silk synthesis approaches, this refined formulation harmonizes the formerly disjointed features yet essential for epidermal electrodes, such as self-adhesiveness, breathability, biodegradability, and elasticity. Therefore, our “soft” electronics merge the best of both “wet” and “dry” electrodes, fostering a conformal skin/electrode interface akin to the wet electrodes while retaining the long-term and irritation-free usage feature of dry electrodes. This achievement is attributed solely to the merger of high self-adhesiveness (300 N/m on glass) and good elasticity (Young’s Modulus of 5.1 kPa and > 600% stretchability) as well as near excellent breathability (1262.6 $g.hour^{-1}.m^{-2}$) of our soft silk electronics which facilitates high fidelity in biosignal recording comparable to the “gold standard” wet Ag/AgCl electrodes.

Indeed, by simultaneously benchmarking our soft electrodes with wet commercial medical-grade electrodes in lead-I electrocardiography (ECG) recording, an almost excellent Pearson’s correlation ratio of 99.4% was achieved, showcasing the feasibility of medical-grade P-QRS-T complex analysis using our soft electrodes. Similarly, signal-to-noise ratio (SNR) values of 9.09 dB (Silk epidermal bioelectronics) compared to 10.08 dB (Ag/AgCl) were observed, verifying the capability for high accuracy biopotential measurements by the developed soft electronics. On the other hand, unlike the gold standard electrodes, our inkjet-printed 200 μm resolution fine patterned solution exhibits high transparency (> 95%) as well as an irritation- and pain-free

operation, devoid of even mild discomfort during removal, rendering them nearly imperceptible during wear, which align seamlessly with the “wear and forget” concept of next generation of *in situ* continuous personalized health monitoring devices. Moreover, we demonstrate robust self-adhered electrode/skin attachment, resisting detachment even under running water or after immersion in a water bath. On the other hand, we also showcase the ease of detachment without causing any discomfort, and our thermal imaging analysis of the skin after five hours of continuous use demonstrates the sustained comfort and absence of irritation throughout wear.

Furthermore, our research demonstrates the extensive capability of our soft electronics in detecting various human electrophysiological signals using identical electrodes and hardware, with the only variation being the placement of the electrodes.This encompasses the recording not only of neural activities in the hundreds of micro-volt range (electroencephalography, EEG) and milli-volt ocular activities (electrooculography, EOG), but also, notably, it can capture cardiac activities in the tens of micro-volt range from EEG signals. This ability to detect such minute signals underscores the superior performance of our electrodes and hardware, further demonstrating their potential for diverse applications in both research and clinical settings.Furthermore, our single-lead EEG recording analysis extends beyond acquiring alpha waves. It also encompasses the recording of beta EEG waves, which is associated with deep meditation or mental arithmetic calculations rarely reported in the context of single-channel EEG.

Therefore, this study presents an all-in-one solution, poised to propel the next generation of epidermal bioelectronics applications, transcending healthcare, wellness, and fitness domains, and maybe introduce novel electrophysiological sensory inputs for emerging augmented and virtual reality platforms whose electrode placement configuration always includes the forehead.

BIBLIOGRAPHY

[1] X. Ma *et al.*, “Stretchable and Skin-Attachable Electronic Device for Remotely Controlled Wearable Cancer Therapy,” *Advanced Science*, vol. 10, no. 10, Apr. 2023, doi: 10.1002/advs.202205343.

[2] A. K. Yetisen, J. L. Martinez-Hurtado, B. Ünal, A. Khademhosseini, and H. Butt, “Wearables in Medicine,” *Advanced Materials*, vol. 30, no. 33, Aug. 2018, doi: 10.1002/adma.201706910.

[3] Y. Chen, Y. Sun, Y. Wei, and J. Qiu, “How Far for the Electronic Skin: From Multifunctional Material to Advanced Applications,” *Adv Mater Technol*, vol. 8, no. 8, Apr. 2023, doi: 10.1002/admt.202201352.

[4] S. Park *et al.*, “Fully Screen-Printed PI/PEG Blends Enabled Patternable Electrodes for Scalable Manufacturing of Skin-Conformal, Stretchable, Wearable Electronics,” *ACS Appl Mater Interfaces*, vol. 15, no. 1, pp. 2092–2103, Jan. 2023, doi: 10.1021/acsami.2c17653.

[5] Y. Li, A. F. Rodríguez-Serrano, S. Y. Yeung, and I. Hsing, “Highly Stretchable and Skin Adhesive Soft Bioelectronic Patch for Long-Term Ambulatory Electrocardiography Monitoring,” *Adv Mater Technol*, vol. 7, no. 6, Jun. 2022, doi: 10.1002/admt.202101435.

[6] S. R. Madhvapathy *et al.*, “Epidermal Electronic Systems for Measuring the Thermal Properties of Human Skin at Depths of up to Several Millimeters,” *Adv Funct Mater*, vol. 28, no. 34, Aug. 2018, doi: 10.1002/adfm.201802083.

[7] G. Kiaee, P. Mostafalu, M. Samandari, and S. Sonkusale, “A pH-Mediated Electronic Wound Dressing for Controlled Drug Delivery,” *Adv Healthc Mater*, vol. 7, no. 18, Sep. 2018, doi: 10.1002/adhm.201800396.

[8] S. R. Madhvapathy *et al.*, “Reliable, low-cost, fully integrated hydration sensors for monitoring and diagnosis of inflammatory skin diseases in any environment,” *Sci Adv*, vol. 6, no. 49, Dec. 2020, doi: 10.1126/sciadv.abd7146.

[9] S. Kwon *et al.*, “At-home wireless sleep monitoring patches for the clinical assessment of sleep quality and sleep apnea,” *Sci Adv*, vol. 9, no. 21, May 2023, doi: 10.1126/sciadv.adg9671.

[10] A. Golparvar, J. Kim, A. Boukhayma, D. Briand, and S. Carrara, “Highly accurate multimodal monitoring of lactate and urea in sweat by soft epidermal optofluidics with single-band Raman scattering,” *Sens Actuators B Chem*, vol. 387, p. 133814, Jul. 2023, doi: 10.1016/j.snb.2023.133814.

[11] L. Beker *et al.*, “A bioinspired stretchable membrane-based compliance sensor,” *Proceedings of the National Academy of Sciences*, vol. 117, no. 21, pp. 11314–11320, May 2020, doi: 10.1073/pnas.1909532117.

[12] S. Lim *et al.*, “Transparent and Stretchable Interactive Human Machine Interface Based on Patterned Graphene Heterostructures,” *Adv Funct Mater*, vol. 25, no. 3, pp. 375–383, Jan. 2015, doi: 10.1002/adfm.201402987.

[13] H. Kang *et al.*, “Fingerprint-Inspired Conducting Hierarchical Wrinkles for Energy-Harvesting E-Skin,” *Adv Funct Mater*, vol. 29, no. 43, Oct. 2019, doi: 10.1002/adfm.201903580.

[14] Y. Liu *et al.*, “Skin-Integrated Graphene-Embedded Lead Zirconate Titanate Rubber for Energy Harvesting and Mechanical Sensing,” *Adv Mater Technol*, vol. 4, no. 12, Dec. 2019, doi: 10.1002/admt.201900744.

[15] H. U. Chung *et al.*, “Binodal, wireless epidermal electronic systems with in-sensor analytics for neonatal intensive care,” *Science (1979)*, vol. 363, no. 6430, Mar. 2019, doi: 10.1126/science.aau0780.

[16] M. J. Bathaei *et al.*, “Photolithography-Based Microfabrication of Biodegradable Flexible and Stretchable Sensors,” *Advanced Materials*, vol. 35, no. 6, Feb. 2023, doi: 10.1002/adma.202207081.

[17] F. Stauffer *et al.*, “Skin Conformal Polymer Electrodes for Clinical ECG and EEG Recordings,” *Adv Healthc Mater*, vol. 7, no. 7, Apr. 2018, doi: 10.1002/adhm.201700994.

[18] H. Li *et al.*, “Breathable and Skin-Conformal Electronics with Hybrid Integration of Microfabricated Multifunctional Sensors and Kirigami-Structured Nanofibrous Substrates,” *Adv Funct Mater*, vol. 32, no. 32, Aug. 2022, doi: 10.1002/adfm.202202792.

[19] S. Wang *et al.*, “Skin electronics from scalable fabrication of an intrinsically stretchable transistor array,” *Nature*, vol. 555, no. 7694, pp. 83–88, Mar. 2018, doi: 10.1038/nature25494.

[20] M. Cai, Z. Jiao, S. Nie, C. Wang, J. Zou, and J. Song, “A multifunctional electronic skin based on patterned metal films for tactile sensing with a broad

linear response range," *Sci Adv*, vol. 7, no. 52, Dec. 2021, doi: 10.1126/sciadv.abl8313.

[21] I. Ibanez Labiano and A. Alomainy, "Flexible inkjet-printed graphene antenna on Kapton," *Flexible and Printed Electronics*, vol. 6, no. 2, p. 025010, Jun. 2021, doi: 10.1088/2058-8585/ac0ac1.

[22] P. He *et al.*, "Screen-Printing of a Highly Conductive Graphene Ink for Flexible Printed Electronics," *ACS Appl Mater Interfaces*, vol. 11, no. 35, pp. 32225–32234, Sep. 2019, doi: 10.1021/acsami.9b04589.

[23] Q. Huang and Y. Zhu, "Gravure Printing of Water-based Silver Nanowire ink on Plastic Substrate for Flexible Electronics," *Sci Rep*, vol. 8, no. 1, p. 15167, Oct. 2018, doi: 10.1038/s41598-018-33494-9.

[24] S. Liang, X. Chen, F. Li, and N. Song, "Laser-Engraved Liquid Metal Circuit for Wearable Electronics," *Bioengineering*, vol. 9, no. 2, p. 59, Jan. 2022, doi: 10.3390/bioengineering9020059.

[25] M. Cai, Z. Jiao, S. Nie, C. Wang, J. Zou, and J. Song, "A multifunctional electronic skin based on patterned metal films for tactile sensing with a broad linear response range," *Sci Adv*, vol. 7, no. 52, Dec. 2021, doi: 10.1126/sciadv.abl8313.

[26] Z. Gao, Z. Lou, W. Han, and G. Shen, "A Self-Healable Bifunctional Electronic Skin," *ACS Appl Mater Interfaces*, vol. 12, no. 21, pp. 24339–24347, May 2020, doi: 10.1021/acsami.0c05119.

[27] Y. Qiao *et al.*, "Intelligent and Multifunctional Graphene Nanomesh Electronic Skin with High Comfort," *Small*, vol. 18, no. 7, Feb. 2022, doi: 10.1002/smll.202104810.

[28] J. Chen, Y. Zhu, and W. Jiang, "A stretchable and transparent strain sensor based on sandwich-like PDMS/CNTs/PDMS composite containing an ultrathin conductive CNT layer," *Compos Sci Technol*, vol. 186, p. 107938, Jan. 2020, doi: 10.1016/j.compscitech.2019.107938.

[29] X.-J. Zha *et al.*, "Nanofibrillar Poly(vinyl alcohol) Ionic Organohydrogels for Smart Contact Lens and Human-Interactive Sensing," *ACS Appl Mater Interfaces*, vol. 12, no. 20, pp. 23514–23522, May 2020, doi: 10.1021/acsami.0c06263.

[30] T. Vuorinen, J. Niittynen, T. Kankkunen, T. M. Kraft, and M. Mäntysalo, "Inkjet-Printed Graphene/PEDOT:PSS Temperature Sensors on a Skin-

Conformable Polyurethane Substrate," *Sci Rep*, vol. 6, no. 1, p. 35289, Oct. 2016, doi: 10.1038/srep35289.

[31] Z. Lei, Q. Wang, S. Sun, W. Zhu, and P. Wu, "A Bioinspired Mineral Hydrogel as a Self-Healable, Mechanically Adaptable Ionic Skin for Highly Sensitive Pressure Sensing," *Advanced Materials*, vol. 29, no. 22, Jun. 2017, doi: 10.1002/adma.201700321.

[32] B. Boubellouta and S. Kusch-Brandt, "Relationship between economic growth and mismanaged e-waste: Panel data evidence from 27 EU countries analyzed under the Kuznets curve hypothesis," *Waste Management*, vol. 120, pp. 85–97, Feb. 2021, doi: 10.1016/j.wasman.2020.11.032.

[33] Mark Rippon, Richard White, and Phil Davies, "Skin adhesives and their role in wound dressings," *Wounds, Uk*, 2007.

[34] S. R. Krishnan *et al.*, "Wireless, Battery-Free Epidermal Electronics for Continuous, Quantitative, Multimodal Thermal Characterization of Skin," *Small*, vol. 14, no. 47, Nov. 2018, doi: 10.1002/smll.201803192.

[35] V. Sanchez-Romaguera *et al.*, "Towards inkjet-printed low cost passive UHF RFID skin mounted tattoo paper tags based on silver nanoparticle inks," *J Mater Chem C Mater*, vol. 1, no. 39, p. 6395, 2013, doi: 10.1039/c3tc31302f.

[36] A. Al-Halhouli, L. Al-Ghussain, S. El Bouri, H. Liu, and D. Zheng, "Fabrication and Evaluation of a Novel Non-Invasive Stretchable and Wearable Respiratory Rate Sensor Based on Silver Nanoparticles Using Inkjet Printing Technology," *Polymers (Basel)*, vol. 11, no. 9, p. 1518, Sep. 2019, doi: 10.3390/polym11091518.

[37] L. Lo, H. Shi, H. Wan, Z. Xu, X. Tan, and C. Wang, "Inkjet-Printed Soft Resistive Pressure Sensor Patch for Wearable Electronics Applications," *Adv Mater Technol*, vol. 5, no. 1, Jan. 2020, doi: 10.1002/admt.201900717.

[38] S. Tonello *et al.*, "Design and in vitro Characterization of a Wearable Multisensing System for Hydration Monitoring," *IEEE Trans Instrum Meas*, vol. 73, pp. 1–11, 2024, doi: 10.1109/TIM.2024.3369161.

[39] B. Krykpayev, M. F. Farooqui, R. M. Bilal, M. Vaseem, and A. Shamim, "A wearable tracking device inkjet-printed on textile," *Microelectronics J*, vol. 65, pp. 40–48, Jul. 2017, doi: 10.1016/j.mejo.2017.05.010.

[40] J. K. Sahoo, O. Hasturk, T. Falcucci, and D. L. Kaplan, “Silk chemistry and biomedical material designs,” *Nat Rev Chem*, vol. 7, no. 5, pp. 302–318, Apr. 2023, doi: 10.1038/s41570-023-00486-x.

[41] D. Zhao, Y. Zhu, W. Cheng, W. Chen, Y. Wu, and H. Yu, “Cellulose-Based Flexible Functional Materials for Emerging Intelligent Electronics,” *Advanced Materials*, vol. 33, no. 28, Jul. 2021, doi: 10.1002/adma.202000619.

[42] J. You, M. Li, B. Ding, X. Wu, and C. Li, “Crab Chitin-Based 2D Soft Nanomaterials for Fully Biobased Electric Devices,” *Advanced Materials*, vol. 29, no. 19, May 2017, doi: 10.1002/adma.201606895.

[43] H.-M. Wang, T.-Q. Yuan, G.-Y. Song, and R.-C. Sun, “Advanced and versatile lignin-derived biodegradable composite film materials toward a sustainable world,” *Green Chemistry*, vol. 23, no. 11, pp. 3790–3817, 2021, doi: 10.1039/D1GC00790D.

[44] M. Jian, Y. Zhang, and Z. Liu, “Natural Biopolymers for Flexible Sensing and Energy Devices,” *Chinese Journal of Polymer Science*, vol. 38, no. 5, pp. 459–490, May 2020, doi: 10.1007/s10118-020-2379-9.

[45] L. Wang, D. Chen, K. Jiang, and G. Shen, “New insights and perspectives into biological materials for flexible electronics,” *Chem Soc Rev*, vol. 46, no. 22, pp. 6764–6815, 2017, doi: 10.1039/C7CS00278E.

[46] G. Chen *et al.*, “Plasticizing Silk Protein for On-Skin Stretchable Electrodes,” *Advanced Materials*, vol. 30, no. 21, May 2018, doi: 10.1002/adma.201800129.

[47] L.-D. Koh *et al.*, “Structures, mechanical properties and applications of silk fibroin materials,” *Prog Polym Sci*, vol. 46, pp. 86–110, Jul. 2015, doi: 10.1016/j.progpolymsci.2015.02.001.

[48] S. Szymkowiak, N. Sandler, and D. L. Kaplan, “Aligned Silk Sponge Fabrication and Perfusion Culture for Scalable Proximal Tubule Tissue Engineering,” *ACS Appl Mater Interfaces*, vol. 13, no. 9, pp. 10768–10777, Mar. 2021, doi: 10.1021/acsami.1c00548.

[49] T. Dong *et al.*, “The regenerated silk fibroin hydrogel with designed architecture bioprinted by its microhydrogel,” *J Mater Chem B*, vol. 7, no. 27, pp. 4328–4337, 2019, doi: 10.1039/C9TB00783K.

[50] S. Mirbakht, A. Golparvar, M. Umar, and M. K. Yapici, “Flexible Silk-Based Graphene Bioelectronics for Wearable Multimodal Physiological Monitoring,” in *2023 IEEE 36th International Conference on Micro Electro Mechanical Systems (MEMS)*, IEEE, Jan. 2023, pp. 335–338. doi: 10.1109/MEMS49605.2023.10052459.

[51] G. Li *et al.*, “Silk-Based Biomaterials in Biomedical Textiles and Fiber-Based Implants,” *Adv Healthc Mater*, vol. 4, no. 8, pp. 1134–1151, Jun. 2015, doi: 10.1002/adhm.201500002.

[52] Z. Wang *et al.*, “Silk Microneedle Patch Capable of On-Demand Multidrug Delivery to the Brain for Glioblastoma Treatment,” *Advanced Materials*, vol. 34, no. 1, Jan. 2022, doi: 10.1002/adma.202106606.

[53] S. Yi *et al.*, “Flat Silk Cocoon-Based Dressing: Daylight-Driven Rechargeable Antibacterial Membranes Accelerate Infected Wound Healing,” *Adv Healthc Mater*, vol. 11, no. 21, Nov. 2022, doi: 10.1002/adhm.202201397.

[54] H. Yang *et al.*, “Adhesive Biocomposite Electrodes on Sweaty Skin for Long-Term Continuous Electrophysiological Monitoring,” *ACS Mater Lett*, vol. 2, no. 5, pp. 478–484, May 2020, doi: 10.1021/acsmaterialslett.0c00085.

[55] G. H. Altman *et al.*, “Silk-based biomaterials,” *Biomaterials*, vol. 24, no. 3, pp. 401–416, Feb. 2003, doi: 10.1016/S0142-9612(02)00353-8.

[56] D. N. Rockwood, R. C. Preda, T. Yücel, X. Wang, M. L. Lovett, and D. L. Kaplan, “Materials fabrication from Bombyx mori silk fibroin,” *Nat Protoc*, vol. 6, no. 10, pp. 1612–1631, Oct. 2011, doi: 10.1038/nprot.2011.379.

[57] D. Umuhoza, F. Yang, D. Long, Z. Hao, J. Dai, and A. Zhao, “Strategies for Tuning the Biodegradation of Silk Fibroin-Based Materials for Tissue Engineering Applications,” *ACS Biomater Sci Eng*, vol. 6, no. 3, pp. 1290–1310, Mar. 2020, doi: 10.1021/acsbiomaterials.9b01781.

[58] M. Biagiotti *et al.*, “Electrospun Silk Fibroin Scaffolds for Tissue Regeneration: Chemical, Structural, and Toxicological Implications of the Formic Acid-Silk Fibroin Interaction,” *Front Bioeng Biotechnol*, vol. 10, Jan. 2022, doi: 10.3389/fbioe.2022.833157.

[59] H. Lyu *et al.*, “Supertough and highly stretchable silk protein-based films with controlled biodegradability,” *Acta Biomater*, vol. 153, pp. 149–158, Nov. 2022, doi: 10.1016/j.actbio.2022.09.010.

[60] H.-J. Jin *et al.*, “Water-Stable Silk Films with Reduced β-Sheet Content,” *Adv Funct Mater*, vol. 15, no. 8, pp. 1241–1247, Aug. 2005, doi: 10.1002/adfm.200400405.

[61] J. Seo, H. Kim, K. Kim, S. Q. Choi, and H. J. Lee, “Calcium-Modified Silk as a Biocompatible and Strong Adhesive for Epidermal Electronics,” *Adv Funct Mater*, vol. 28, no. 36, Sep. 2018, doi: 10.1002/adfm.201800802.

[62] S.-P. Sinikumpu, J. Jokelainen, S. Keinänen-Kiukaanniemi, and L. Huilaja, “Skin cancers and their risk factors in older persons: a population-based study,” *BMC Geriatr*, vol. 22, no. 1, p. 269, Dec. 2022, doi: 10.1186/s12877-022-02964-1.

[63] D. Wilborn, J. Kottner, K. Hillmann, S. Xu, F. Konietschke, and U. Blume-Peytavi, “Interrelationships between Skin Structure, Function, and Microbiome of Pregnant Females and Their Newborns: Study Protocol for a Prospective Cohort Study,” *Dermatol Res Pract*, vol. 2021, pp. 1–10, Nov. 2021, doi: 10.1155/2021/4163705.

[64] I. M. F. de Souza, G. L. N. Vitral, M. V. Caliari, and Z. S. N. Reis, “Association between the chronology of gestation and the morphometrical skin characteristics at childbirth: a development of predictive model,” *BMJ Health Care Inform*, vol. 28, no. 1, p. e100476, Dec. 2021, doi: 10.1136/bmjhci-2021-100476.

[65] Q. Wang, S. Ling, X. Liang, H. Wang, H. Lu, and Y. Zhang, “Self-Healable Multifunctional Electronic Tattoos Based on Silk and Graphene,” *Adv Funct Mater*, vol. 29, no. 16, p. 1808695, Apr. 2019, doi: 10.1002/adfm.201808695.

[66] Q. Li *et al.*, “Highly Thermal-Wet Comfortable and Conformal Silk-Based Electrodes for On-Skin Sensors with Sweat Tolerance,” *ACS Nano*, vol. 15, no. 6, pp. 9955–9966, Jun. 2021, doi: 10.1021/acsnano.1c01431.

[67] X. Yan *et al.*, “Highly breathable, surface-hydrophobic and wet-adhesive silk based epidermal electrode for long-term electrophysiological monitoring,” *Compos Sci Technol*, vol. 230, p. 109751, Nov. 2022, doi: 10.1016/j.compscitech.2022.109751.

[68] L. Meng, Q. Fu, S. Hao, F. Xu, and J. Yang, “Self-adhesive, biodegradable silk-based dry electrodes for epidermal electrophysiological

monitoring," *Chemical Engineering Journal*, vol. 427, p. 131999, Jan. 2022, doi: 10.1016/j.cej.2021.131999.

[69] N. Gogurla, Y. Kim, S. Cho, J. Kim, and S. Kim, "Multifunctional and Ultrathin Electronic Tattoo for On-Skin Diagnostic and Therapeutic Applications," *Advanced Materials*, vol. 33, no. 24, Jun. 2021, doi: 10.1002/adma.202008308.

[70] J. Huang *et al.*, "Tuning the Rigidity of Silk Fibroin for the Transfer of Highly Stretchable Electronics," *Adv Funct Mater*, vol. 30, no. 23, Jun. 2020, doi: 10.1002/adfm.202001518.

[71] M. Jo *et al.*, "Protein-Based Electronic Skin Akin to Biological Tissues," *ACS Nano*, vol. 12, no. 6, pp. 5637–5645, Jun. 2018, doi: 10.1021/acsnano.8b01435.

[72] K. Wang, U. Parekh, T. Pailla, H. Garudadri, V. Gilja, and T. N. Ng, "Stretchable Dry Electrodes with Concentric Ring Geometry for Enhancing Spatial Resolution in Electrophysiology," *Adv Healthc Mater*, vol. 6, no. 19, Oct. 2017, doi: 10.1002/adhm.201700552.

[73] M. Reis Carneiro, C. Majidi, and M. Tavakoli, "Multi-Electrode Printed Bioelectronic Patches for Long-Term Electrophysiological Monitoring," *Adv Funct Mater*, vol. 32, no. 43, Oct. 2022, doi: 10.1002/adfm.202205956.

[74] Y. Yamamoto *et al.*, "Efficient Skin Temperature Sensor and Stable Gel-Less Sticky ECG Sensor for a Wearable Flexible Healthcare Patch," *Adv Healthc Mater*, vol. 6, no. 17, Sep. 2017, doi: 10.1002/adhm.201700495.

[75] L. Tian *et al.*, "Large-area MRI-compatible epidermal electronic interfaces for prosthetic control and cognitive monitoring," *Nat Biomed Eng*, vol. 3, no. 3, pp. 194–205, Feb. 2019, doi: 10.1038/s41551-019-0347-x.

[76] S. Mishra *et al.*, "Soft, wireless periocular wearable electronics for real-time detection of eye vergence in a virtual reality toward mobile eye therapies," *Sci Adv*, vol. 6, no. 11, Mar. 2020, doi: 10.1126/sciadv.aay1729.

[77] W. Zhou, S. Yao, H. Wang, Q. Du, Y. Ma, and Y. Zhu, "Gas-Permeable, Ultrathin, Stretchable Epidermal Electronics with Porous Electrodes," *ACS Nano*, vol. 14, no. 5, pp. 5798–5805, May 2020, doi: 10.1021/acsnano.0c00906.

[78] Y. Li *et al.*, "A Stretchable-Hybrid Low-Power Monolithic ECG Patch with Microfluidic Liquid-Metal Interconnects and Stretchable Carbon-Black

Nanocomposite Electrodes for Wearable Heart Monitoring," *Adv Electron Mater*, vol. 5, no. 2, Feb. 2019, doi: 10.1002/aelm.201800463.

[79] Y. Ling *et al.*, "Skin-Inspired Porous Mesh Bioelectronics with Built-In Multifunctionality for Concurrently Monitoring Heart Electrical and Mechanical Functions," *Adv Funct Mater*, vol. 33, no. 41, Oct. 2023, doi: 10.1002/adfm.202302681.

[80] Y. Kim *et al.*, "All-in-One, Wireless, Stretchable Hybrid Electronics for Smart, Connected, and Ambulatory Physiological Monitoring," *Advanced Science*, vol. 6, no. 17, Sep. 2019, doi: 10.1002/advs.201900939.

[81] Y. Zhao *et al.*, "Ultra-conformal skin electrodes with synergistically enhanced conductivity for long-time and low-motion artifact epidermal electrophysiology," *Nat Commun*, vol. 12, no. 1, p. 4880, Aug. 2021, doi: 10.1038/s41467-021-25152-y.

[82] L. Zhang *et al.*, "Fully organic compliant dry electrodes self-adhesive to skin for long-term motion-robust epidermal biopotential monitoring," *Nat Commun*, vol. 11, no. 1, p. 4683, Sep. 2020, doi: 10.1038/s41467-020-18503-8.

[83] Q. Tian *et al.*, "Hairy-Skin-Adaptive Viscoelastic Dry Electrodes for Long-Term Electrophysiological Monitoring," *Advanced Materials*, vol. 35, no. 30, Jul. 2023, doi: 10.1002/adma.202211236.

[84] Y. Hao *et al.*, "A Stretchable, Breathable, And Self-Adhesive Electronic Skin with Multimodal Sensing Capabilities for Human-Centered Healthcare," *Adv Funct Mater*, vol. 33, no. 44, Oct. 2023, doi: 10.1002/adfm.202303881.

[85] Q. Wang, S. Ling, X. Liang, H. Wang, H. Lu, and Y. Zhang, "Self-Healable Multifunctional Electronic Tattoos Based on Silk and Graphene," *Adv Funct Mater*, vol. 29, no. 16, Apr. 2019, doi: 10.1002/adfm.201808695.

[86] Y. Hao *et al.*, "A Stretchable, Breathable, And Self-Adhesive Electronic Skin with Multimodal Sensing Capabilities for Human-Centered Healthcare," *Adv Funct Mater*, vol. 33, no. 44, Oct. 2023, doi: 10.1002/adfm.202303881.

[87] C. Pailler-Mattei, S. Bec, and H. Zahouani, "In vivo measurements of the elastic mechanical properties of human skin by indentation tests," *Med Eng Phys*, vol. 30, no. 5, pp. 599–606, Jun. 2008, doi: 10.1016/j.medengphy.2007.06.011.

[88] M. Geerligs, L. van Breemen, G. Peters, P. Ackermans, F. Baaijens, and C. Oomens, "In vitro indentation to determine the mechanical properties of

epidermis," *J Biomech*, vol. 44, no. 6, pp. 1176–1181, Apr. 2011, doi: 10.1016/j.jbiomech.2011.01.015.

[89] G. Acar, O. Ozturk, A. J. Golparvar, T. A. Elboshra, K. Böhringer, and M. K. Yapici, "Wearable and Flexible Textile Electrodes for Biopotential Signal Monitoring: A review," *Electronics (Basel)*, vol. 8, no. 5, p. 479, Apr. 2019, doi: 10.3390/electronics8050479.

[90] X. Cai, J. Lin, and S. Wang, "Novel Peptide with Specific Calcium-Binding Capacity from Schizochytrium sp. Protein Hydrolysates and Calcium Bioavailability in Caco-2 Cells," *Mar Drugs*, vol. 15, no. 1, p. 3, Dec. 2016, doi: 10.3390/md15010003.

[91] G. Zhang, L. Wang, and J. Pan, "Probing the Binding of the Flavonoid Diosmetin to Human Serum Albumin by Multispectroscopic Techniques," *J Agric Food Chem*, vol. 60, no. 10, pp. 2721–2729, Mar. 2012, doi: 10.1021/jf205260g.

[92] Y. Ji *et al.*, "DFT-Calculated IR Spectrum Amide I, II, and III Band Contributions of *N* -Methylacetamide Fine Components," *ACS Omega*, vol. 5, no. 15, pp. 8572–8578, Apr. 2020, doi: 10.1021/acsomega.9b04421.

[93] G. Hu *et al.*, "Isolation, Purification and Structure Identification of a Calcium-Binding Peptide from Sheep Bone Protein Hydrolysate," *Foods*, vol. 11, no. 17, p. 2655, Sep. 2022, doi: 10.3390/foods11172655.

[94] J. Seo, H. Kim, K. Kim, S. Q. Choi, and H. J. Lee, "Calcium-Modified Silk as a Biocompatible and Strong Adhesive for Epidermal Electronics," *Adv Funct Mater*, vol. 28, no. 36, Sep. 2018, doi: 10.1002/adfm.201800802.

[95] F. Zhang, X. You, H. Dou, Z. Liu, B. Zuo, and X. Zhang, "Facile Fabrication of Robust Silk Nanofibril Films via Direct Dissolution of Silk in $CaCl_2$ –Formic Acid Solution," *ACS Appl Mater Interfaces*, vol. 7, no. 5, pp. 3352–3361, Feb. 2015, doi: 10.1021/am508319h.

[96] Q. Lu *et al.*, "Water-insoluble silk films with silk I structure," *Acta Biomater*, vol. 6, no. 4, pp. 1380–1387, Apr. 2010, doi: 10.1016/j.actbio.2009.10.041.

[97] K. Luo, Y. Yang, and Z. Shao, "Physically Crosslinked Biocompatible Silk-Fibroin-Based Hydrogels with High Mechanical Performance," *Adv Funct Mater*, vol. 26, no. 6, pp. 872–880, Feb. 2016, doi: 10.1002/adfm.201503450.

[98] Q. Xie *et al.*, “Transparent, Flexible, and Stable Polyethersulfone/Copper-Nanowires/Polyethylene Terephthalate Sandwich-Structured Films for High-Performance Electromagnetic Interference Shielding,” *Adv Eng Mater*, vol. 23, no. 8, Aug. 2021, doi: 10.1002/adem.202100283.

[99] R. D. Rodriguez *et al.*, “Ultra-Robust Flexible Electronics by Laser-Driven Polymer-Nanomaterials Integration,” *Adv Funct Mater*, vol. 31, no. 17, Apr. 2021, doi: 10.1002/adfm.202008818.

[100] Z. Yang *et al.*, “Wearable electronics for heating and sensing based on a multifunctional PET/silver nanowire/PDMS yarn,” *Nanoscale*, vol. 12, no. 31, pp. 16562–16569, 2020, doi: 10.1039/D0NR04023A.

[101] L. Liu, K. Kuffel, D. K. Scott, G. Constantinescu, H.-J. Chung, and J. Rieger, “Silicone-based adhesives for long-term skin application: cleaning protocols and their effect on peel strength,” *Biomed Phys Eng Express*, vol. 4, no. 1, p. 015004, Nov. 2017, doi: 10.1088/2057-1976/aa91fb.

[102] A. Chen *et al.*, “Self-adhesive electronic skin for ultra-sensitive healthcare monitoring,” *J Mater Chem A Mater*, vol. 11, no. 10, pp. 4977–4986, 2023, doi: 10.1039/D2TA08628J.

[103] R. A. Nawrocki, H. Jin, S. Lee, T. Yokota, M. Sekino, and T. Someya, “Self-Adhesive and Ultra-Conformable, Sub-300 nm Dry Thin-Film Electrodes for Surface Monitoring of Biopotentials,” *Adv Funct Mater*, vol. 28, no. 36, Sep. 2018, doi: 10.1002/adfm.201803279.

[104] S. Wang, J. Xiao, H. Liu, and L. Zhang, “Silk nanofibrous iontronic sensors for accurate blood pressure monitoring,” *Chemical Engineering Journal*, vol. 453, p. 139815, Feb. 2023, doi: 10.1016/j.cej.2022.139815.

[105] S. Yoon, M. Seok, M. Kim, and Y.-H. Cho, “Wearable porous PDMS layer of high moisture permeability for skin trouble reduction,” *Sci Rep*, vol. 11, no. 1, p. 938, Jan. 2021, doi: 10.1038/s41598-020-78580-z.

[106] Y. Kambe, Y. Mizoguchi, K. Kuwahara, T. Nakaoki, Y. Hirano, and T. Yamaoka, “Beta-sheet content significantly correlates with the biodegradation time of silk fibroin hydrogels showing a wide range of compressive modulus,” *Polym Degrad Stab*, vol. 179, p. 109240, Sep. 2020, doi: 10.1016/j.polymdegradstab.2020.109240.

[107] G. Li *et al.*, “PEDOT:PSS/Grafted-PDMS Electrodes for Fully Organic and Intrinsically Stretchable Skin-like Electronics,” *ACS Appl Mater Interfaces*, vol. 11, no. 10, pp. 10373–10379, Mar. 2019, doi: 10.1021/acsami.8b20255.

[108] Y.-W. Cai *et al.*, “Self-healable, super-stretchable and shape-adaptive triboelectric nanogenerator based on double cross-linked PDMS for electronic skins,” *Nano Energy*, vol. 102, p. 107683, Nov. 2022, doi: 10.1016/j.nanoen.2022.107683.

[109] P. Gokhale *et al.*, “Controlling the crack formation in inkjet-printed silver nanoparticle thin-films for high resolution patterning using intense pulsed light treatment,” *Nanotechnology*, vol. 28, no. 49, p. 495301, Dec. 2017, doi: 10.1088/1361-6528/aa9238.

[110] W. Ahmed and S. Khalid, “ECG signal processing for recognition of cardiovascular diseases: A survey,” in *2016 Sixth International Conference on Innovative Computing Technology (INTECH)*, IEEE, Aug. 2016, pp. 677–682. doi: 10.1109/INTECH.2016.7845089.

[111] M. K. Yapici, T. Alkhidir, Y. A. Samad, and K. Liao, “Graphene-clad textile electrodes for electrocardiogram monitoring,” *Sens Actuators B Chem*, vol. 221, pp. 1469–1474, Dec. 2015, doi: 10.1016/j.snb.2015.07.111.

[112] S. Cheng *et al.*, “Ultrathin Hydrogel Films toward Breathable Skin-Integrated Electronics,” *Advanced Materials*, vol. 35, no. 1, Jan. 2023, doi: 10.1002/adma.202206793.

[113] A. J. Golparvar and M. K. Yapici, “Toward graphene textiles in wearable eye tracking systems for human–machine interaction,” *Beilstein Journal of Nanotechnology*, vol. 12, pp. 180–189, Feb. 2021, doi: 10.3762/bjnano.12.14.

[114] S. Ban *et al.*, “Soft Wireless Headband Bioelectronics and Electrooculography for Persistent Human–Machine Interfaces,” *ACS Appl Electron Mater*, vol. 5, no. 2, pp. 877–886, Feb. 2023, doi: 10.1021/acsaelm.2c01436.

[115] A. Golparvar, O. Ozturk, and M. K. Yapici, “Gel-Free Wearable Electroencephalography (EEG) with Soft Graphene Textiles,” in *2021 IEEE Sensors*, IEEE, Oct. 2021, pp. 1–4. doi: 10.1109/SENSORS47087.2021.9639711.